

# Anomaly, Class Division, and Decoupling in Wealth Dynamics

Jaeseok Hur,<sup>1</sup> Meesoon Ha,<sup>2,\*</sup> and Hawoong Jeong<sup>1,3,†</sup>

<sup>1</sup>*Department of Physics, Korea Advanced Institute of Science and Technology, Daejeon 34141, Korea*

<sup>2</sup>*Department of Physics Education, Chosun University, Gwangju, 61452, Korea*

<sup>3</sup>*Center of Complex Systems, KAIST, Daejeon 34141, Korea*

(Dated: July 11, 2025)

Economic inequality is driven by the structure of agent networks, interactions among agents, and the abilities of individual agents. We provide a comprehensive picture of anomalous diffusion, economic class division, and bimodal wealth distribution in an agent-based model, where heterogeneous agent abilities and growth rates are tuned on sparse regular networks. In particular, we focus on the statistical characteristics of logarithmic scaled normalized wealth distributions with two ability parameters, assortativity  $\mathcal{A}$  and concentration  $\mathcal{R}$ . For the set of  $(\mathcal{A}, \mathcal{R})$ , temporal behaviors of log-wealth distributions reveal that the decoupling between different ability groups depends primarily on  $\mathcal{R}$  and long-term inequality depends mainly on  $\mathcal{A}$ . In other words, class division and decoupling are driven by  $\mathcal{R}$ , while the super-diffusive nature in the leading class is driven by  $\mathcal{A}$ . Our findings highlight that hierarchical segregation of abilities, rather than ability differences alone, is a key driver of economic class stratification. Finally, our model provides a minimal, yet powerful framework for understanding the bimodal global income distribution observed over the past half century and highlights the critical role of network-level segregation in shaping economic inequality.

Since the book by Piketty [1], *Capital in the Twenty-First Century*, sparked a debate on the mechanism of economic inequality, the distribution of income in wealth dynamics has been widely studied by theoretical [2–8] and empirical [9–19]. In *World Inequality Report 2022* [20], global income inequality for the period 1950–2010 was explained by differences in countries [10, 17]. Such an inequality was represented by the Gini coefficient/index, peaked at the end of the twentieth century, resulting in a bimodal global income distribution. In addition, strong regional correlations were also found in the income levels of the countries [21], and the corresponding regional convergence has been studied by [22–24].

As the simplest agent-based model by Bouchaud and Mézard (BM) [25] studied the capital trade between agents and wealth condensation. The original BM model is described by a stochastic differential equation (SDE)

$$dC_n = \alpha C_n dt + \beta C_n dW_{t,n} + \sum_{m(\neq n)} (J_{nm} C_m - J_{mn} C_n) dt, \quad (1)$$

where  $n$  is agent index,  $C_n$  is the wealth (capital) of agent  $n$ ,  $dt$  is time interval,  $W_{t,n}$  is Wiener process of  $n$  at time  $t$ ,  $\alpha$  is the percentage drift (ability),  $\beta$  is the percentage volatility, and  $J_{nm}$  is the element of an interaction matrix  $\mathbf{J}$ , respectively. Initially, all agents have the same capital. This equation follows the Itô interpretation.

To focus on the relative wealth of agents, we introduce a normalized wealth  $c \equiv C/\bar{C}$  where  $\bar{C}$  is an average wealth, and rewrite Eq. (1) by proper notations [26] as

$$dc_n = J \sum_{\{m|a_{nm}=1\}} \left( \frac{c_m}{k_m} - \frac{c_n}{k_n} \right) dt + \beta c_n dW_{t,n}, \quad (2)$$

where  $a_{mn}$  is the element of the adjacency matrix  $\mathbf{a}$  for an agent-based network, and the strength of the interaction between agent  $n$  and  $m$  is  $J_{nm} = J/k_m$  with a constant  $J$  and the degree of agent  $m$ ,  $k_m$ . The normalized wealth distribution  $\rho(c)$  has been investigated [27–34] for various network topologies, such as regular lattices, small-world [35], and scale-free [36] networks.

However, temporal behaviors and anomalies of  $\rho(c)$  have rarely been discussed. For a sparse regular network with an average degree  $k$  that is small enough, it was reported that  $\rho(c)$  follows a log-normal [27, 29], but no clear explanation is available for the origin of the log-normality. In addition, the bimodality and polarization of  $\rho(c)$  cannot be realized by models with homogeneous abilities, where  $\rho(c)$  is unimodal.

In this Letter, we focus on anomalous behaviors and class division of wealth-levels with decoupling in wealth dynamics. To provide a possible mechanism for wealth-level segregation, we modify the BM model for a one-dimensional (1D) ring topology with a binary mixture of abilities. In particular, we investigate the effect of ability configuration on the bimodality of log-wealth distributions, in the context of two relevant parameters that control the ability configuration, see Fig. 1 and the Supplemental Material (SM) [37] for the more detailed investigation. As a result, we address the 1D ring topology and ability configuration to be key ingredients for strong regional correlation and polarization of income levels.

The ordinary BM model with homogeneous abilities is formulated in a regular network as follows:

$$dc_n = J(\bar{c}_n^{(k)} - c_n) dt + \beta c_n dW_{t,n}, \quad (3)$$

where  $\bar{c}_n^{(k)}$  is the average normalized wealth of  $n$ 's neighbors with the average degree  $k$ . In order to solve Eq. (3),

we use the effective field theory (EFT) ansatz [33] for  $\bar{c}_n^{(k)} \rightarrow \theta(\eta)c_n^{1-\eta}$  with a field exponent  $\eta \in [0, 1]$  and a normalization factor  $\theta(\eta)$  from  $\langle c \rangle = 1$ .

For a 1D ring topology, the wealth values of neighboring agents become similar to each other,  $c_n \simeq c_{n\pm 1}$  until the detailed balance condition is preserved, except for fluctuations. Because the 1D ring can be considered for the minimally connected case, the corresponding  $\eta$  is expected to be small. Based on the essence of the EFT ansatz, the SDE depends only on  $c_n$  as

$$dc_n = J[\theta(\eta)c_n^{1-\eta} - c_n]dt + \beta c_n dW_{t,n}. \quad (4)$$

Let  $x \equiv \ln c$  and assume that  $\eta x$  is sufficiently small, then the first-order approximation becomes a time-dependent Ornstein-Uhlenbeck (OU) process [38] as

$$dx_n = J\eta\theta(\eta) \left[ \left( \frac{\theta(\eta) - 1}{\eta\theta(\eta)} \right) - x_n \right] dt - \frac{\beta^2}{2} dt + \beta dW_{t,n}, \quad (5)$$

where  $\eta$  and  $\theta(\eta)$  depend on  $t$ . Surprisingly, for large  $t$ , the variance of the process of Eq. (5) is asymptotically similar to that of the ordinary OU process [39], where both  $\eta$  and  $\theta$  are substituted as constants. This phenomenon depends on the slow decay of  $\eta(t)$ . Hence,  $\rho(x, t) \approx \rho_{\text{eq}}^{(\text{OU})}(x, t; \eta, \theta)$ . If the EFT ansatz is in good approximation, the random variables of  $Y = \ln \bar{c}^{(k)}$  and  $X = \ln c$  have a linear relationship as  $Y = (1 - \eta)X + \ln \theta(\eta)$ . According to the least square linear regression, we empirically find that  $\eta$  follows time-asymptotic power-law as  $\eta(t) \sim a_0 t^{-\lambda}$  for large  $t$  with constant  $a_0$  and  $0.5 \leq \lambda < 1$ , as well as  $\theta(\eta) \rightarrow 1$  for large  $t$ , which satisfies the prediction of the EFT that  $\eta$  is very small for a sparse regular network. This supports our approximation that  $\rho(x, t) \approx \rho_{\text{eq}}^{(\text{OU})}(x, t; \eta, \theta)$  at each point in time is approximately Gaussian. For large  $t$ , the variance  $\sigma_t^2 = \beta^2 t^\lambda / (2J a_0)$  and the mean  $\mu_t = -\sigma_t^2 / 2$  of  $\langle c \rangle = 1$ , such that  $c_t \sim \text{Lognormal}(\mu_t, \sigma_t^2)$ .

To investigate long-range correlations, we take the 1D ring topology under the small  $\beta$  condition. Then, the SDE for  $X$  corresponds to the multidimensional OU process, and the interaction matrix is marginally stable [40]. For such a case, we express the covariance of agents in range  $\ell$  ( $\ell = 1, 2, \dots$ ) as

$$\text{Cov}(X_n, X_{n+\ell}) = \beta^2 \int_0^t e^{-2Js} I_\ell(2Js) ds, \quad (6)$$

where  $I_\ell$  is the modified Bessel function of the first kind. For the same time  $t$ , the shorter distance  $\ell$  the larger the covariance. The results in strong regional correlations of  $X$  that make the clustering of rich and poor agents as shown in Fig. 1 (b) and (c), respectively. It is noted that  $\eta(t) \sim a_0 t^{-1/2}$  for large  $t$ , see SM [37] for the detailed derivation of  $\text{Var}(X)$ ,  $\text{Cov}(X, Y)$ ,  $\eta(t)$ , and correlations.

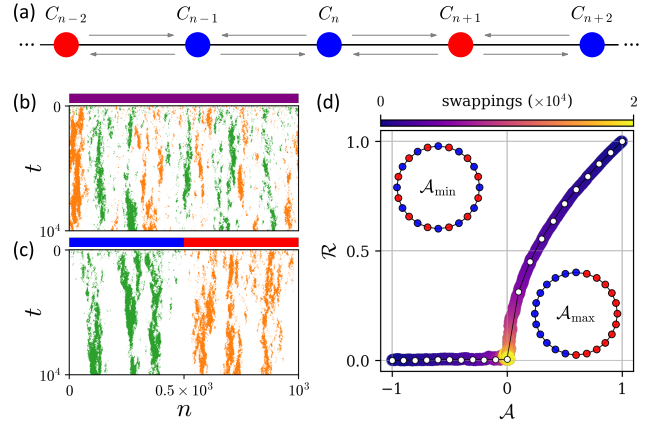


FIG. 1. (a) Schematic illustration of BM wealth dynamics with a binary mixture of agent abilities:  $\bullet$  ( $\alpha_+$ ) and  $\bullet$  ( $\alpha_-$ ) for  $\alpha_{\pm} = \alpha \pm \Delta\alpha$  and wealth ( $C$ ) transfer (either  $\rightarrow$  or  $\leftarrow$ ) between two nearest-neighboring agents. Dynamics of top/bottom 10% (orange/green) class for two extreme configurations, (b)  $\mathcal{A}_{\min}$  and (c)  $\mathcal{A}_{\max}$ : The agent index  $n$  is shown in horizontal from left to right, and time  $t$  is in vertical from top to bottom. Here  $N = 10^3$ ,  $\alpha = 10^{-2}$ ,  $\Delta\alpha = 10^{-3}$ ,  $\beta^2 = 10^{-3}$ , and  $J = 10^{-1}$  in Eq. (7). The snapshot is taken in a single run. (d) Random pair swapping trajectories of  $(\mathcal{A}, \mathcal{R})$ . The path starts from two extreme configurations with  $(\mathcal{A}_{\min/\max}, \mathcal{R}_{\min/\max})$  (see insets). Each pair swapping trial is represented by color gradation. Simulation samples (c) are chosen with 0.1 interval in  $[\mathcal{A}_{\min}, \mathcal{A}_{\max}]$ .

For heterogeneous wealth dynamics, we consider the percentage growth rate  $\alpha$  as an ability to generate wealth. For simplicity, we employ a binary mixture of abilities in the BM model for the 1D ring topology. The following SDE is for the heterogeneous BM (HBM) model:

$$dC_n = \alpha_n C_n dt + \beta C_n dW_{t,n} + J(\bar{C}_n^{(k)} - C_n) dt, \quad (7)$$

where  $\alpha_n = \alpha \pm \Delta\alpha$ . It is noted that  $\alpha$  and  $\Delta\alpha$  are both positive constants satisfying  $\alpha > \Delta\alpha$ . The SDE given in Eq. (7) is implemented in a quenched disorder, since once the configuration has been selected, it does not change over time. The disorder in the ability configuration breaks the translational invariance of the system, and the transformation in Eq. (2) does not hold. As a result, for the HBM model, the wealth dynamics is also influenced by the ability configuration. Without loss of generality, we only consider when the number of agents for the  $\alpha_+$  group is the same as that for the other  $\alpha_-$  group, *i.e.*,  $N_+ = N_-$ , where  $\alpha_{\pm} = \alpha \pm \Delta\alpha$  (see Fig. 1).

To speculate on all possible configurations, we quantify the statistical properties of the  $\alpha$  configuration, in terms of two relevant parameters. The first parameter  $\mathcal{A}$  is an ability assortativity that represents how many similar  $\alpha$  values are connected for a given network:

$$\mathcal{A} \equiv \frac{\text{Cov}(\alpha, \alpha')}{\sqrt{\text{Var}(\alpha)\text{Var}(\alpha')}}, \quad (8)$$

where  $\alpha$  and  $\alpha'$  are the abilities of the agents connected for a given network. For the binary mixture in the 1D ring and the case of  $N_+ = N_-$ , it is simply  $\mathcal{A} = \rho^{(1)} - \rho^{(2)}$ , where  $\rho^{(1)}$  and  $\rho^{(2)}$  are homogeneous and heterogeneous link densities, respectively. The actual bounds [41] of  $\mathcal{A}$  depend on the topology of the network [42]. For the 1D ring topology, the alternative allocation of abilities becomes the lower bound of  $\mathcal{A}$ , and the fully separated allocation becomes the upper bound of  $\mathcal{A}$ . As a result,  $\mathcal{A}_{\min} = -1$  and  $\mathcal{A}_{\max} = +1 - N/4$ , see insets in Fig. 1 (d).

In Fig. 1 (d), the second parameter  $\mathcal{R}$  is derived from the phase order parameter in the Kuramoto model [43, 44], which represents the concentration of positional ability in the 1D ring. Thus,  $(r_{\pm}, \psi_{\pm})$  is  $r_{\pm}e^{i\psi_{\pm}} = \frac{1}{N_{\pm}} \sum_j e^{i\phi_j^{(\pm)}}$ , where  $\phi_j^{(\pm)}$  is the angular argument for binary ability groups, respectively. In the HBM model, all agents are assigned in the 1D ring with the same intervals. Thus,  $\phi_j = 2\pi m/N$ , where  $m \in \{0, \dots, N-1\}$ . For the case of  $N_+ = N_-$  and  $r_{\pm} \neq 0$ , two important quantities become  $r_+ = r_- = r$  and  $\Delta\psi = |\psi_+ - \psi_-| = \pi$ . For every configuration,  $\Delta\psi$  is either  $\pi$  or not defined ( $r = 0$ ), so we only need to consider  $r$ . For the perfectly disassortative case with  $\mathcal{A}_{\min}$  and the perfectly assortative case with  $\mathcal{A}_{\max}$ ,  $r \rightarrow 0$  and  $r \rightarrow 2/\pi$  as  $N \rightarrow \infty$ , which are the minimum and the maximum. Hence,  $\mathcal{R}$  is defined as a statistical control parameter:

$$\mathcal{R} \equiv r/[(2/\pi)]. \quad (9)$$

Estimating dynamic properties in the 1D HBM model with decoupling and inequality, we employ two statistical measures, the Hellinger distance  $h$  [45, 46] and the Gini index  $g$  [47, 48]. First,  $h$  is defined as

$$h(\rho_1, \rho_2) \equiv \sqrt{\frac{1}{2} \int \left( \sqrt{\rho_1(x)} - \sqrt{\rho_2(x)} \right)^2 dx} \quad (10)$$

where  $0 \leq h \leq 1$ ,  $\rho_1$  and  $\rho_2$  are probability distributions. This representation follows the Lebesgue measure. The entire  $\rho(x, t)$  can be decomposed by the distributions of  $\alpha_{\pm}$  groups (see Figs. 1 and 2):

$$\rho(x, t) = [\rho_{\alpha_-}(x, t) + \rho_{\alpha_+}(x, t)]/2.$$

It is noted that  $h(\rho_{\alpha_-}, \rho_{\alpha_+})$  is either 0 for the perfectly coupled state or 1 for the perfectly decoupled state (see Fig. 2). Second,  $g$  for  $c$  is defined as

$$g \equiv \frac{1}{2} \int_0^{\infty} \int_0^{\infty} \rho(c)\rho(c')|c - c'|dc dc' \quad (11)$$

where  $0 \leq g \leq 1$ ,  $g = 0$  represents perfect equality, and  $g = 1$  does extreme inequality as the wealth condensation state with the whole wealth monopolized by a few agents.

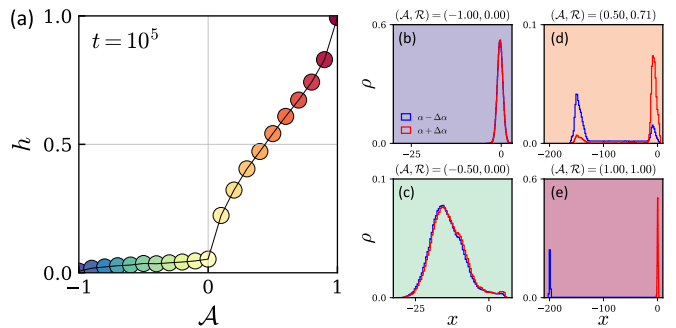


FIG. 2. Configuration effect on decoupling: (a) Hellinger distance  $h$  in Eq. (10) plotted at  $t = 10^5$  against  $\mathcal{A}$  with  $\mathcal{R}(\mathcal{A})$  [see Fig. 1(d)]. Selected snapshots for unimodal and bimodal distributions: (b), (c), (d), and (e) are the cases of  $(\mathcal{A}, \mathcal{R}) = (-1.00, 0.00)$ ,  $(-0.50, 0.00)$ ,  $(0.50, 0.71)$ , and  $(1.00, 1.00)$ , respectively. Here the model parameters,  $N$ , and the number of ensembles are the same as Fig. 1.

In process of sampling the ability configuration, we use the random pair swapping algorithm: (i) Start from two extreme configurations:  $(\mathcal{A}_{\min}, \mathcal{R}_{\min})$ ,  $(\mathcal{A}_{\max}, \mathcal{R}_{\max})$ . (ii) Select random pairs of nodes and switch positions. If this process is repeated for large iterations,  $(\mathcal{A}, \mathcal{R})$  almost converges to near  $(0, 0)$ .

To figure out the effect of the ability configuration on wealth dynamics at a glance, we compare two extreme cases of ability configurations,  $\mathcal{A}_{\min}$  and  $\mathcal{A}_{\max}$ . For the perfectly disassortative case,  $\rho(x, t; \mathcal{A}_{\min})$  is

$$\rho(x, t; \mathcal{A}_{\min}) \approx \rho_{\alpha_{\pm}}(x, t) \sim \mathcal{N}(\mu_t, \sigma_t^2), \quad (12)$$

where  $\sigma_t^2 = \beta^2 t^\lambda / (2Ja_0)$  and  $\mu_t = -\sigma_t^2/2$  for large  $t$ . Such results are inherited from the BM model for a 1D ring topology. It shows  $h \approx 0$  that  $\rho_{\alpha_{\pm}}$  is almost perfectly overlapped with each other, see Fig. 2 (b). In other words, the perfectly disassortative configuration neutralizes the impact of heterogeneous agent abilities.

For the perfectly assortative case,  $\rho(x, t; \mathcal{A}_{\max})$  for large  $t$  can be divided into three parts: (i) Gaussian peak around the first mode (head),  $\rho^{(h)}$ ; (ii) Flat region between the two peaks (intermediate/body),  $\rho^{(b)}$ ; (iii) Gaussian peak around the second mode (tail),  $\rho^{(t)}$ , see SM [37] for detailed analyses and numerical confirmations. It is noted that  $\rho^{(h)}$  and  $\rho^{(t)}$  are formed by lower and higher ability agents, respectively. The segregation of wealth level between two groups increases linearly in  $t$ ,  $\Delta\mu = \langle x_{\alpha_+ \Delta\alpha} \rangle - \langle x_{\alpha_- \Delta\alpha} \rangle \approx 2\Delta\alpha t$ . The motions in the same ability group are described by the sub-diffusive nature represented by  $\sigma_t^2$ , but the relative motion between different groups  $\alpha_{\pm}$  is described by the ballistic motion represented by  $\Delta\mu$ . Since  $\Delta\mu$  increases faster than  $\sigma_t$ , there is almost no overlap between  $\rho_{\pm}$  for large  $t$  and it shows  $h \approx 1$ . In other words, the perfectly assortative configuration maximizes wealth-level decoupling.

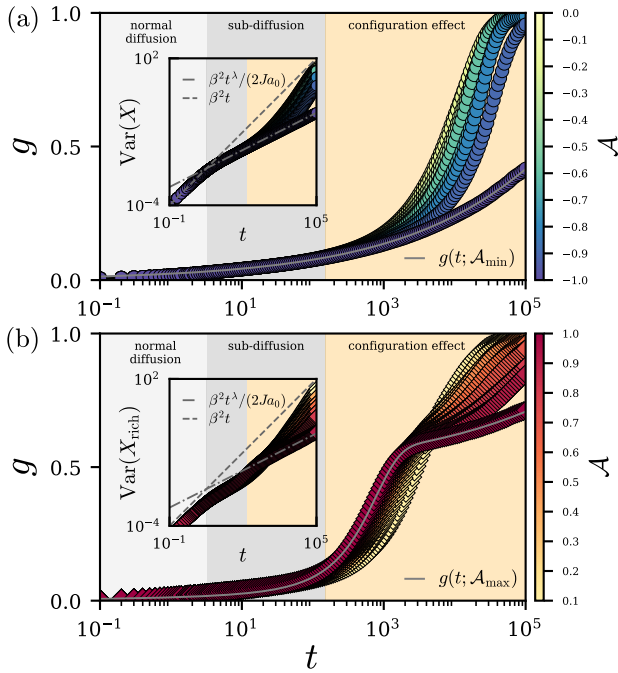


FIG. 3. Configuration effect on inequality by Gini coefficient  $g$  against  $t$ : Each color reflects the selected samples of  $\mathcal{A}$  with  $\mathcal{R}$  in Fig. 1(d). (a) Path 1 -  $(\mathcal{A}_{\min}, \mathcal{R}_{\min}) \rightarrow (0, 0)$  and (b) Path 2 -  $(\mathcal{A}_{\max}, \mathcal{R}_{\max}) \rightarrow (0, 0)$ , respectively. As  $t$  elapses, the system undergoes from normal diffusion (below  $t = 10$ ) to configuration effect (above  $t = 10^2$ ) via the sub-diffusion regime. The insets of (a) and (b) are  $\text{Var}(X)$  and  $\text{Var}(X_{\text{rich}})$ , respectively. The guided lines are shown for normal diffusion and sub-diffusion as described.

For the perfectly disassortative case,  $g(t; \mathcal{A}_{\min})$  is

$$g(t; \mathcal{A}_{\min}) \approx \text{erf}(\sigma_t/2). \quad (13)$$

The increase of  $g(t)$  is driven by sub-diffusion because there is almost no decoupling between  $\rho_{\alpha_{\pm}}(x, t)$ . For the perfectly assortative case,  $g(t; \mathcal{A}_{\max})$  is

$$g(t; \mathcal{A}_{\max}) \approx \frac{1}{2} \left( 1 - \frac{2}{1 + e^{2\Delta\alpha t}} \right) + \frac{1}{2} \text{erf}(\sigma_t/2), \quad (14)$$

where the segregation of wealth-level makes the  $\alpha_-$  group hold almost no share of wealth. Thus, the cumulative share of  $c$  up to the 50% of population is almost 0. The first term of Eq. (14) reflects the inequality between  $\alpha_{\pm}$  groups and converges to 1/2 very quickly due to the segregation of wealth-levels between them. The second term reflects inequality within the  $\alpha_+$  group and converges to 1/2 very slowly because of the sub-diffusive nature in the Gaussian peak. This is a considerable example that shows the decomposed impact of between and within inequalities on the entire inequality.

Lastly, the time evolution of  $g$  is shown in Fig. 3, which is complicated. For all configurations, the system exhibits three different diffusion regimes: (i) Normal diffusion;

(ii) Gaussian sub-diffusion; (iii) Non-Gaussian diffusion. The first and second regimes are inherited from the BM model, but the third regime is the unique feature of the HBM model, emerging from ability configuration effects.

At *path 1*, both  $\rho_+$  and  $\rho_-$  overlap with each other [see Fig. 2 (b) and (c)], and only diffusion determines inequality. Thus,  $g$  follows a single time scale as described in Eq.(13). For this case, the larger  $\mathcal{A}$ , the larger  $g$ . At *path 2*,  $\rho_+$  and  $\rho_-$  are divided [see Fig. 2 (d) and (e)], so that both class division and diffusion determine inequality. Once two classes are divided into poor and rich ones, the poor class holds almost no share of wealth, resulting in  $g \rightarrow 1/2$  as Eq.(14). On the other hand, half of  $g$  remains determined by diffusion in the rich class. Thus,  $g$  has dual-time scales that indicate crossover regimes in  $g$ , and one should consider  $\text{Var}(X_{\text{rich}})$  separately, where  $X_{\text{rich}}$  is larger than the median of  $X$ . In Fig. 3 (b), we show that the smaller  $\mathcal{A}$ , the larger  $\text{Var}(X_{\text{rich}})$ . It results in fast condensation ( $g \rightarrow 1$ ). In short,  $\mathcal{R}$  drives class division and  $g$  exceeds 1/2 quickly as  $\mathcal{R}$  increases, whereas  $\mathcal{A} \rightarrow 0$  lets the system be super-diffusive and  $g$  eventually approaches 1 more rapidly. It is surprising that by introducing a modest degree of ability heterogeneity and mixing it up on the 1D ring, a super-diffusive nature is emerged because it does not happen in the former model.

In summary, our minimal model study has realized the bimodality of the global income distribution in the 20th century. In particular, it provided three remarks that make our case more plausible: (i) Log-normality [49]; (ii) Strong autocorrelation [50]; (iii) Strong regional correlations and segregation [51]. Our model could be extended to more complex network topologies, which is beyond the scope of our study, but represents a compelling avenue for future work. Finally, our results highlight the significant impact of the ability allocation on the individual's economic growth, compared to the Hotelling's model [52] and the most recent study on the spatio-temporal distribution of housing prices [53]. For simplicity, we chose a binary mixture of abilities, which can be considered with the continuous spectrum. The distributions of GDP growth rates and stock returns follow Laplace or Student's t-distribution [54–56], which can be described by introducing specific continuous ability spectrum. The impact of heterogeneity and continuity of abilities on wealth dynamics has also been studied in [57, 58]. The similar approach with volatility  $\beta$  can be established as well. Finally, to describe the global income distribution under more realistic bases, the approach with temporal networks could be a possible candidate [59].

This research was supported by Basic Science Research Program through the National Research Foundation of Korea (NRF) (KR) [NRF-2020R1A2C1007703 (J.H., M.H.) and NRF-RS-2025-00514776 (J.H., H.J.)].

- \* [msha@chosun.ac.kr](mailto:msha@chosun.ac.kr)  
† [hjeong@kaist.edu](mailto:hjeong@kaist.edu)
- [1] T. Piketty, *Trans. Arthur Goldhammer/Belknap* (2014).
  - [2] R. Gibrat, *Sirey* (1931).
  - [3] P. Pestieau and U. M. Possen, *Econometrica: Journal of the Econometric Society*, 761 (1979).
  - [4] P. Pestieau and U. M. Possen, *European Economic Review* **17**, 279 (1982).
  - [5] D. Chotikapanich, *Modeling income distributions and Lorenz curves*, Vol. 5 (Springer Science & Business Media, 2008).
  - [6] B. K. Chakrabarti, A. Chakraborti, S. R. Chakravarty, and A. Chatterjee, *Econophysics of income and wealth distributions* (Cambridge University Press, 2013).
  - [7] M. Nirei and S. Aoki, *Review of Economic Dynamics* **20**, 25 (2016).
  - [8] X. Gabaix, J.-M. Lasry, P.-L. Lions, and B. Moll, *Econometrica* **84**, 2071 (2016).
  - [9] T. Piketty and E. Saez, *The Quarterly journal of economics* **118**, 1 (2003).
  - [10] F. Bourguignon and C. Morrisson, *American economic review* **92**, 727 (2002).
  - [11] X. Sala-i Martin, *The quarterly journal of economics* **121**, 351 (2006).
  - [12] M. Pinkovskiy and X. Sala-i Martin, *Parametric estimations of the world distribution of income*, Tech. Rep. (National Bureau of Economic Research, 2009).
  - [13] S. Anand and P. Segal, *Journal of economic literature* **46**, 57 (2008).
  - [14] J. L. Van Zanden, J. Baten, P. Foldvari, and B. Van Leeuwen, *Review of income and wealth* **60**, 279 (2014).
  - [15] P. Liberati, *Review of Income and Wealth* **61**, 248 (2015).
  - [16] B. Milanovic, *World Bank Policy Research Working Paper* (2012).
  - [17] B. Milanovic, *Review of Economics and Statistics* **97**, 452 (2015).
  - [18] C. Lakner and B. Milanovic, *The World Bank Economic Review* **30**, 203 (2016).
  - [19] M. Roser, *Our World in Data* (2017), <https://ourworldindata.org/the-history-of-global-economic-inequality>.
  - [20] L. Chancel, T. Piketty, E. Saez, and G. Zucman, *World inequality report 2022* (Harvard University Press, 2022).
  - [21] M. Roser, B. Rohenkohl, P. Arriagada, J. Hasell, H. Ritchie, and E. Ortiz-Ospina, *Data page: World bank income groups*, <https://ourworldindata.org/grapher/world-bank-income-groups> (2023), part of the publication: "Economic Growth". Data adapted from World Bank.
  - [22] S. J. Rey and B. D. Montouri, *Regional studies* **33**, 143 (1999).
  - [23] G. Arbia and G. Piras, (2005).
  - [24] D. Yamamoto, *Journal of Economic Geography* **8**, 79 (2008).
  - [25] J.-P. Bouchaud and M. Mézard, *Physica A: Statistical Mechanics and its Applications* **282**, 536 (2000).
  - [26] By using  $\bar{C} = C(0)e^{\alpha t}$ , we get  $dc_n = d(C_n/\bar{C}) = dC_n/\bar{C} - (C_n/\bar{C}^2)d\bar{C} = dC_n/\bar{C} - \alpha c_n dt$  in Eq. (2).
  - [27] W. Souma, Y. Fujiwara, and H. Aoyama, *arXiv preprint cond-mat/0108482* (2001).
  - [28] W. Souma, Y. Fujiwara, and H. Aoyama, in *Meeting the Challenge of Social Problems via Agent-Based Simulation: Post-Proceedings of the Second International Workshop on Agent-Based Approaches in Economic and Social Complex Systems* (Springer, 2003) pp. 37–49.
  - [29] D. Garlaschelli and M. I. Loffredo, *Physica A: Statistical Mechanics and its Applications* **338**, 113 (2004).
  - [30] D. Garlaschelli and M. I. Loffredo, *Journal of Physics A: Mathematical and Theoretical* **41**, 224018 (2008).
  - [31] M. Medo, *Journal of Statistical Mechanics: Theory and Experiment* **2009**, P02014 (2009).
  - [32] T. Ichinomiya, *Physical Review E—Statistical, Nonlinear, and Soft Matter Physics* **88**, 012819 (2013).
  - [33] T. Ma, J. G. Holden, and R. Serota, *Physica A: Statistical Mechanics and its Applications* **392**, 2434 (2013).
  - [34] T. Ichinomiya, *Physical Review E—Statistical, Nonlinear, and Soft Matter Physics* **86**, 036111 (2012).
  - [35] D. J. Watts and S. H. Strogatz, *Nature* **393**, 440 (1998).
  - [36] A.-L. Barabási and R. Albert, *Science* **286**, 509 (1999).
  - [37] See Supplemental Material at [URL will be inserted by publisher] for more details, which includes Refs [22–25, 31, 33, 40, 60–62].
  - [38] C. W. Gardiner *et al.*, *Handbook of stochastic methods*, Vol. 3 (springer Berlin, 1985).
  - [39] In the ordinary OU process,  $\rho_{\text{eq}}^{\text{(OU)}}(x)$  is a Gaussian with variance  $\sigma^2$  that converges to the ratio of the diffusion coefficient to the dissipation factor,  $\sigma^2 \rightarrow \beta^2/[2J\eta\theta(\eta)]$ .
  - [40] J.-P. Bouchaud, *arXiv preprint arXiv:2407.10284* (2024).
  - [41] The value of the Pearson correlation coefficient is bounded between -1 and 1.
  - [42] M. Cinelli, L. Peel, A. Iovanella, and J.-C. Delvenne, *Physical Review E* **102**, 062310 (2020).
  - [43] Y. Kuramoto, *Lecture notes in Physics* **30**, 420 (1975).
  - [44] S. H. Strogatz, *Physica D: Nonlinear Phenomena* **143**, 1 (2000).
  - [45] E. Hellinger, *Journal für die reine und angewandte Mathematik* **1909**, 210 (1909).
  - [46] M. S. Nikulin *et al.*, *Encyclopedia of mathematics* **78** (2001).
  - [47] C. Gini, *Variabilità e mutabilità: contributo allo studio delle distribuzioni e delle relazioni statistiche.[Fasc. I.]* (Tipogr. di P. Cuppini, 1912).
  - [48] C. Gini, *General series* **208** (1936).
  - [49] It is known that income distribution has log-normality only except super riches [2, 6, 63]. The empirical estimation [12, 15, 64] for each country is based on the log-normal assumption.
  - [50] Income levels of countries have persistent behavior [20, 65, 66]. In the 1D BM model, the autocorrelation coefficient [60] (ACC) exhibit time asymptotic power law decay and long memory property in contrast to the geometric Brownian motion and the mean field BM model that show exponential decay of ACC.
  - [51] GDP per capita and income is spatially correlated and their regional convergence is studied by [21–24]. In the HBM model, regional segregation of income levels is driven by large  $\mathcal{R}$ , implying that spatial concentration of infrastructures and economic opportunities may form strong regional dependency of income levels [16, 17].
  - [52] H. Hotelling, in *The Foundations of Price Theory Vol 4* (Routledge, 2024) pp. 241–260.
  - [53] A.-C. Becharat, M. Benzaquen, and J.-P. Bouchaud, *arXiv preprint arXiv:2412.14624* (2024).

- [54] M. A. Williams, G. Baek, Y. Li, L. Y. Park, and W. Zhao, *Physica A: Statistical Mechanics and Its Applications* **468**, 750 (2017).
- [55] E. Platen and R. Rendek, *Journal of statistical theory and practice* **2**, 233 (2008).
- [56] A. Chakraborti, I. M. Toke, M. Patriarca, and F. Abergel, *Quantitative Finance* **11**, 991 (2011).
- [57] A. Pluchino, A. E. Biondo, and A. Rapisarda, *Advances in Complex systems* **21**, 1850014 (2018).
- [58] J. Hur, M. Ha, and H. Jeong, *Physical Review E* **110**, 024312 (2024).
- [59] Because the declining of global income Gini index in 21th century relies on the structure based changes on economy around the world such as growth rate increase in China and developing countries [15] and evolution of network structure on the world trade web [67, 68].
- [60] K. I. Park, M. Park, *et al.*, *Fundamentals of probability and stochastic processes with applications to communications* (Springer, 2018).
- [61] F. Lillo and J. D. Farmer, *Studies in nonlinear dynamics & econometrics* **8**, 20123001 (2004).
- [62] P. A. Moran, *Biometrika* **37**, 17 (1950).
- [63] W. Souma, in *Empirical science of financial fluctuations: the advent of econophysics* (Springer, 2002) pp. 343–352.
- [64] D. Chotikapanich, R. Valenzuela, and D. Prasada Rao, *Empirical Economics* **22**, 533 (1997).
- [65] S. N. Durlauf, *Journal of Economic growth* **1**, 75 (1996).
- [66] J. Blanden, P. Gregg, and L. Macmillan, *The Economic Journal* **117**, C43 (2007).
- [67] M. Á. Serrano, M. Boguñá, and A. Vespignani, *Journal of Economic Interaction and Coordination* **2**, 111 (2007).
- [68] M.-Y. Cha, J. W. Lee, and D.-S. Lee, *Journal of the Korean Physical Society* **56**, 998 (2010).

**SUPPLEMENTAL MATERIAL FOR  
“ANOMALY, CLASS DIVISION, AND DECOUPLING IN WEALTH DYNAMICS”**

**I. BOUCHAUD-MÉZARD MODEL FOR 1D RING TOPOLOGY**

**A. Variance, Covariance, and Field Exponent**

For a one-dimensional (1D) ring topology, Eq. (2) in the main text can be rewritten as

$$dc_n = J \left( \frac{c_{n-1} + c_{n+1}}{2} - c_n \right) dt + \beta c_n dW_{t,n}, \quad (\text{S1})$$

where  $n = 0, 1, \dots, N-1$ . The system satisfies periodic boundary conditions, *i.e.*,  $c_{-1} = c_{N-1}$  and  $c_N = c_0$ .

Define a new variable  $X_n = \ln c_n + \beta^2 t/2$ . Under the condition of small  $\beta$ , we assume that the differences in  $X$  between neighboring agents are sufficiently small. Applying a first-order approximation, Eq. (S1) is transformed into:

$$dX_n = J \left( \frac{X_{n-1} + X_{n+1}}{2} - X_n \right) dt + \beta dW_{t,n}. \quad (\text{S2})$$

To solve the stochastic differential equation (SDE) in Eq. (S2), we apply the discrete Fourier transform:

$$\hat{X}_k = \frac{1}{\sqrt{N}} \sum_{n=0}^{N-1} X_n e^{-i2\pi \frac{k}{N} n}, \quad X_n = \frac{1}{\sqrt{N}} \sum_{k=0}^{N-1} \hat{X}_k e^{i2\pi \frac{k}{N} n}. \quad (\text{S3})$$

Substituting the inverse transform into Eq. (S2), we obtain:

$$d\hat{X}_k(t) = -J \left( 1 - \cos \frac{2\pi k}{N} \right) \hat{X}_k(t) dt + \beta dW_k(t), \quad (\text{S4})$$

which is the SDE corresponding to the  $k$ -th Fourier mode, and where we show that  $\hat{X}_k(t)$  follows an independent *Ornstein-Uhlenbeck* (OU) process for each of the  $k$  modes. The solution of this SDE is

$$\hat{X}_k(t) = \hat{X}_k(0) e^{-Jt(1 - \cos 2\pi k/N)} + \beta \int_0^t e^{-J(1 - \cos 2\pi k/N)(t-s)} dW_k(s). \quad (\text{S5})$$

According to Parseval's Theorem  $\sum_{n=0}^{N-1} |X_n|^2 = \sum_{k=0}^{N-1} |\hat{X}_k|^2$ , the variance of  $X_n$  is as follows:

$$\text{Var}(X_n) = \frac{1}{N} \sum_{n=0}^{N-1} \mathbb{E}[|X_n|^2] - \left( \frac{1}{N} \sum_{n=0}^{N-1} \mathbb{E}[X_n] \right)^2 = \frac{1}{N} \sum_{k=0}^{N-1} \mathbb{E}[|\hat{X}_k|^2] - \left( \frac{1}{N} \sum_{n=0}^{N-1} \mathbb{E}[X_n] \right)^2. \quad (\text{S6})$$

Let  $\mathbb{E}[\cdot]$  denote the expectation for the stochastic process. We consider the initial condition,  $X_n(0) = \text{const}$ , where all agents have the same value of  $X$ . From the given SDE, since  $d\left(\sum_{n=0}^{N-1} X_n\right) = 0$ , the mean value of  $X_n$  is always constant, regardless of  $t$ . For this case,  $\hat{X}_k(0) = \frac{1}{\sqrt{N}} \sum_{n=0}^{N-1} X_n(0) e^{-i2\pi \frac{k}{N} n} = \sqrt{N} X_n(0) \delta_{0k}$ . Calculate  $\mathbb{E}[|\hat{X}_k|^2]$  to get  $\text{Var}(X_n)$ .

$$\begin{aligned} \mathbb{E}[|\hat{X}_k|^2] &= \hat{X}_k^2(0) e^{-2Jt(1-\cos 2\pi k/N)} + 2\beta \hat{X}_k(0) e^{-Jt(1-\cos 2\pi k/N)} \int_0^t e^{-J(1-\cos 2\pi k/N)(t-s)} \langle dW_k(s) \rangle \\ &\quad + \beta^2 \int_0^t \int_0^t e^{-2J(1-\cos 2\pi k/N)(t-\frac{s+s'}{2})} \langle dW_k(s) dW_k(s') \rangle \\ &= \hat{X}_k^2(0) e^{-2Jt(1-\cos 2\pi k/N)} + \beta^2 \int_0^t e^{-2J(1-\cos 2\pi k/N)(t-s)} ds \\ &= N X_n^2(0) \delta_{0k} e^{-2Jt(1-\cos 2\pi k/N)} + \beta^2 \left[ \frac{1 - e^{-2Jt(1-\cos 2\pi k/N)}}{2J(1-\cos 2\pi k/N)} \right]. \end{aligned} \quad (\text{S7})$$

where the following properties  $\langle dW_k(s) \rangle = 0$ ,  $\langle dW_k(s) dW_k(s') \rangle = \delta(s-s') ds$ , and  $\delta_{0k}^2 = \delta_{0k}$  are used. Thus,

$$\begin{aligned} \text{Var}(X_n) &= \left[ \frac{1}{N} \sum_{k=0}^{N-1} N X_n(0)^2 \delta_{0k} e^{-2Jt(1-\cos 2\pi k/N)} + \frac{1}{N} \sum_{k=0}^{N-1} \beta^2 \left[ \frac{1 - e^{-2Jt(1-\cos 2\pi k/N)}}{2J(1-\cos 2\pi k/N)} \right] \right] - [X_n(0)^2] \\ &= \frac{1}{N} \sum_{k=0}^{N-1} \beta^2 \left[ \frac{1 - e^{-2Jt(1-\cos 2\pi k/N)}}{2J(1-\cos 2\pi k/N)} \right] \approx \frac{\beta^2}{4\pi J} \int_0^{2\pi} \frac{1 - e^{-2Jt(1-\cos u)}}{1 - \cos u} du = \frac{\beta^2}{2\pi J} \int_0^\pi \frac{1 - e^{-2Jt(1-\cos u)}}{1 - \cos u} du, \end{aligned} \quad (\text{S8})$$

which is the result that transforms the discrete sum of  $k$ -Fourier modes to definite integral as  $N \rightarrow \infty$ , and the periodic property of the integrand allows us to reduce the integration interval  $[0, 2\pi]$  to  $[0, \pi]$ . If we differentiate the above mathematical expression with respect to  $t$ ,

$$\frac{d}{dt} \text{Var}(X_n) = \beta^2 e^{-2Jt} \cdot \frac{1}{\pi} \int_0^\pi e^{2Jt \cos u} du = \beta^2 e^{-2Jt} I_0(2Jt), \quad (\text{S9})$$

where  $I_\ell(z)$  is the modified Bessel function of the first kind. It represents

$$I_\ell(z) = \frac{1}{\pi} \int_0^\pi e^{z \cos \theta} \cos \ell \theta d\theta - \frac{\sin \ell \pi}{\pi} \int_0^\infty e^{-z \cosh q - \ell q} dq. \quad (\text{S10})$$

By solving the differential equation in Eq. (S9), we get  $\text{Var}(X_n)$ . The right-hand side function has a well-defined indefinite integral as follows:

$$\int e^{-2Jt} I_0(2Jt) dt = t e^{-2Jt} [I_0(2Jt) + I_1(2Jt)] + C. \quad (\text{S11})$$

According to initial condition,  $X_n(0) = \text{const}$ , for  $t = 0$ ,  $\text{Var}(X_n(0)) = 0$  and  $\lim_{t \rightarrow 0} t e^{-2Jt} [I_0(2Jt) + I_1(2Jt)] = 0$ . Thus, the constant of integration  $C = 0$ . Therefore, the variance of  $X_n$  is

$$\text{Var}(X_n) = \beta^2 t e^{-2Jt} [I_0(2Jt) + I_1(2Jt)]. \quad (\text{S12})$$

Taylor expansions of Eq. (S12) for small  $t$  and large  $t$  are as follows:

$$\beta^2 t \left( 1 - \frac{(2Jt)}{2} + \frac{(2Jt)^2}{4} - \frac{5(2Jt)^3}{48} + \dots \right) \quad (\text{S13})$$

$$\beta^2 t \left( \sqrt{\frac{2}{\pi}} (2Jt)^{-1/2} - \frac{1}{4\sqrt{2\pi}} (2Jt)^{-3/2} - \frac{3}{64\sqrt{2\pi}} (2Jt)^{-5/2} - \dots \right), \quad (\text{S14})$$

where the leading-order terms are  $\beta^2 t$  and  $\beta^2 \sqrt{t}/(2Ja_0)$ , respectively. It is noted that  $a_0(J) = \sqrt{\pi/(4J)}$ . To sum up,

$$\text{Var}(X_n) = \begin{cases} \beta^2 t & \text{for small } t \\ \beta^2 \sqrt{t}/(2Ja_0) & \text{for large } t \end{cases}. \quad (\text{S15})$$

Thus, the stochastic process in Eq. (S2) starts with normal diffusion and ends with sub-diffusion. For large  $t$ ,  $\text{Var}(X_n) \sim \sqrt{t}$ , and this analytical result is consistent with the EFT and numerical simulations. To obtain  $\eta$ , we need to calculate  $\text{Cov}(X_n, \bar{X}_n)$ . First, the discrete Fourier transform for  $\bar{X}_n$  is

$$\begin{aligned} \hat{X}_k &= \frac{1}{\sqrt{N}} \sum_{n=0}^{N-1} \bar{X}_n e^{-i2\pi \frac{k}{N} n} = \frac{1}{\sqrt{N}} \sum_{n=0}^{N-1} \frac{X_{n-1} + X_{n+1}}{2} e^{-i2\pi \frac{k}{N} n} \\ &= \frac{1}{2\sqrt{N}} \sum_{n=0}^{N-1} \left[ \frac{1}{\sqrt{N}} \sum_{k'=0}^{N-1} (\hat{X}_{k'} e^{i2\pi \frac{k'}{N} (n-1)} + \hat{X}_{k'} e^{i2\pi \frac{k'}{N} (n+1)}) \right] e^{-i2\pi \frac{k}{N} n} \\ &= \frac{1}{2\sqrt{N}} \sum_{n=0}^{N-1} \left[ \frac{1}{\sqrt{N}} \sum_{k'=0}^{N-1} \hat{X}_{k'} e^{i2\pi \frac{k'}{N} n} (e^{-i2\pi \frac{k'}{N}} + e^{i2\pi \frac{k'}{N}}) \right] e^{-i2\pi \frac{k}{N} n} \\ &= \frac{1}{\sqrt{N}} \sum_{n=0}^{N-1} \left[ \frac{1}{\sqrt{N}} \sum_{k'=0}^{N-1} \cos\left(\frac{2\pi k'}{N}\right) \hat{X}_{k'} e^{i2\pi \frac{k'}{N} n} \right] e^{-i2\pi \frac{k}{N} n} = \frac{1}{N} \sum_{k'=0}^{N-1} \cos\left(\frac{2\pi k'}{N}\right) \hat{X}_{k'} \left[ \sum_{n=0}^{N-1} e^{-i2\pi (\frac{k-k'}{N}) n} \right] \\ &= \frac{1}{N} \sum_{k'=0}^{N-1} \cos\left(\frac{2\pi k'}{N}\right) \hat{X}_{k'} N \delta_{kk'} = \cos\left(\frac{2\pi k}{N}\right) \hat{X}_k. \end{aligned} \quad (\text{S16})$$

Substituting this result into the Parseval's theorem, we have

$$\sum_{n=0}^{N-1} X_n \bar{X}_n^* = \sum_{k=0}^{N-1} \hat{X}_k \hat{X}_k^* = \sum_{k=0}^{N-1} \cos\left(\frac{2\pi k}{N}\right) |\hat{X}_k|^2, \quad (\text{S17})$$

where  $X^*$  denotes the complex conjugate of  $X$ . Then, the covariance between  $X_n$  and  $\bar{X}_n$  is

$$\begin{aligned} \text{Cov}(X_n, \bar{X}_n) &= \frac{1}{N} \sum_{n=0}^{N-1} \mathbb{E}[X_n \bar{X}_n^*] - \left( \frac{1}{N} \sum_{n=0}^{N-1} \mathbb{E}[X_n] \right) \left( \frac{1}{N} \sum_{n=0}^{N-1} \mathbb{E}[\bar{X}_n] \right) \\ &= \frac{1}{N} \sum_{k=0}^{N-1} \cos\left(\frac{2\pi k}{N}\right) \mathbb{E}[|\hat{X}_k|^2] - \left( \frac{1}{N} \sum_{n=0}^{N-1} \mathbb{E}[X_n] \right) \left( \frac{1}{N} \sum_{n=0}^{N-1} \mathbb{E}[\bar{X}_n] \right). \end{aligned} \quad (\text{S18})$$

By repeating the procedure that we derived  $\text{Var}(X_n)$ , we get

$$\text{Cov}(X_n, \bar{X}_n) = \frac{\beta^2}{2\pi J} \int_0^\pi \cos u \left[ \frac{1 - e^{-2Jt(1-\cos u)}}{1 - \cos u} \right] du. \quad (\text{S19})$$

The time derivative of Eq. (S19) is

$$\frac{d}{dt} \text{Cov}(X_n, \bar{X}_n) = \beta^2 e^{-2Jt} I_1(2Jt). \quad (\text{S20})$$

The indefinite integral is

$$\begin{aligned} \int d[\text{Cov}(X_n, \bar{X}_n)] &= \beta^2 \int e^{-2Jt} I_1(2Jt) dt = \beta^2 \int e^{-2Jt} (1/2J) \left[ \frac{d}{dt} I_0(2Jt) \right] dt \\ &= \frac{\beta^2}{2J} \left[ e^{-2Jt} I_0(2Jt) + 2J \int e^{-2Jt} I_0(2Jt) dt \right] = \frac{\beta^2}{2J} e^{-2Jt} I_0(2Jt) + \beta^2 \int e^{-2Jt} I_0(2Jt) dt \\ &= \frac{\beta^2}{2J} e^{-2Jt} I_0(2Jt) + \text{Var}(X_n) + C. \end{aligned} \quad (\text{S21})$$

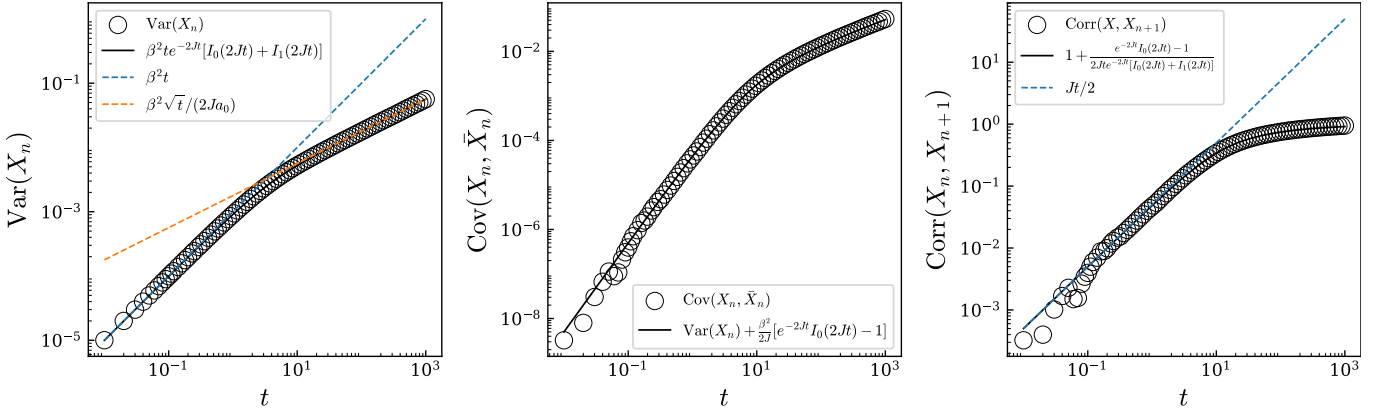


FIG. S1.  $\text{Var}(X_n)$ ,  $\text{Cov}(X_n, \bar{X}_n)$ , and  $\text{Corr}(X_n, X_{n+1})$  of BM model on 1D ring. All hollow dots represent numerical simulation results and solid line represent theoretical prediction. The blue dashed lines  $\{\beta^2 t, Jt/2\}$  are prediction for small  $t$  and the orange dashed line  $\{\beta^2 \sqrt{t}/(2Ja_0)\}$  is prediction for large  $t$ . For all cases, we used  $J = 0.1, \beta = \sqrt{0.001}, N = 10^4$  and ensemble average of 128 runs.

Since the initial condition  $\text{Cov}(X_n(0), \bar{X}_n(0)) = 0$  and  $\lim_{t \rightarrow 0} e^{-2Jt} I_0(2Jt) = 1$  give  $C = -\frac{\beta^2}{2J}$ , the covariance is

$$\text{Cov}(X_n, \bar{X}_n) = \text{Var}(X_n) + \frac{\beta^2}{2J} [e^{-2Jt} I_0(2Jt) - 1]. \quad (\text{S22})$$

Moreover, the correlation between  $X_n$  and  $X_{n+1}$  is as follows:

$$\text{Corr}(X_n, X_{n+1}) \equiv \frac{\text{Cov}(X_n, X_{n+1})}{\sqrt{\text{Var}(X_n)\text{Var}(X_{n+1})}} = \frac{\text{Cov}(X_n, \bar{X}_n)}{\text{Var}(X_n)}, \quad (\text{S23})$$

where  $\text{Cov}(X_n, \bar{X}_n) = (1/2)[\text{Cov}(X_n, X_{n-1}) + \text{Cov}(X_n, X_{n+1})] = \text{Cov}(X_n, X_{n+1})$  and  $\text{Var}(X_n) = \text{Var}(X_{n+1})$  since the system is translational invariant. For small  $t$ , since  $c \simeq 1 + x$ ,  $\text{Var}(X_n) \simeq \text{Var}(c_n)$  and  $\text{Cov}(X_n, \bar{X}_n) \simeq \text{Cov}(c, \bar{c}_n)$ . For a general network, the linear increase in the variance and the correlation is revealed by Medo [31]. Our theory for the BM model in the 1D ring supports this result. Furthermore, it predicts the variance, the covariance, and the correlation for large  $t$ . From the results of  $\text{Var}(X_n)$  and  $\text{Cov}(X_n, \bar{X}_n)$ ,

$$1 - \eta = \frac{\text{Cov}(X_n, \bar{X}_n)}{\text{Var}(X_n)} = \frac{\text{Var}(X_n) + \frac{\beta^2}{2J} [e^{-2Jt} I_0(2Jt) - 1]}{\text{Var}(X_n)} = 1 + \frac{e^{-2Jt} I_0(2Jt) - 1}{2Jte^{-2Jt} [I_0(2Jt) + I_1(2Jt)]}. \quad (\text{S24})$$

Finally, a field exponent  $\eta(t)$  is as follows:

$$\eta(t) = \frac{1 - e^{-2Jt} I_0(2Jt)}{2Jte^{-2Jt} [I_0(2Jt) + I_1(2Jt)]}. \quad (\text{S25})$$

Since  $\eta(t) = -\frac{\beta^2}{2J} \frac{I_0(2Jt)}{t[I_0(2Jt) + I_1(2Jt)]} + \frac{\beta^2}{2J} \frac{1}{\text{Var}(X_n)}$  and  $\lim_{t \rightarrow \infty} \frac{I_0(2Jt)}{t[I_0(2Jt) + I_1(2Jt)]} = 0$ , for large  $t$ ,  $\eta(t) \approx \frac{\beta^2}{2J} \frac{2Ja_0}{\beta^2} t^{-1/2} = a_0 t^{-1/2}$ , which matches our numerical simulation results for the small  $\beta$  condition (see Fig. S2).

Figure S2 shows the time evolution of  $\eta$  for various  $J, \beta$ , and  $k$ . For small  $\beta$ , Eq. (S25) tells us that the power-law decay exponent  $\lambda = 1/2$  is independent of  $J$ . Since  $a_0(J) = \sqrt{\pi/(4J)}$ , an increase in  $J$  only has the effect of parallel shifting  $\eta$  on the double logarithmic plot. However, for large  $\beta$ ,  $\lambda$  is larger than  $1/2$ . In this case, the difference in  $X$  between neighbors cannot be approximated to the first order because it is more affected by multiplicative noise in Eq. (S1). Thus, the variance grows faster than the order of  $\sqrt{t}$ . Varying the number of neighbors  $k$  changes the underlying equation, so that  $X_n$  follows completely different dynamics. For the same setup of  $(J, \beta)$ , the larger  $k$  makes  $\eta$  decrease much more slowly. If  $k$  is large enough,  $\lim_{t \rightarrow \infty} \eta(t)$  converges to a non-zero value, implying that the inequality limit of the system exists, unlike in the case of a ring topology. Ma *et al.* [33] showed that for this case, the equilibrium distribution  $\rho_{\text{eq}}(c)$  satisfying the Fokker-Planck equation is the generalized inverse-gamma distribution.

We conclude this subsection with a discussion on the mean of  $x$ . In fact, deterministic drifts to all  $X_n$  only give the translation to the probability density function, but do not change its shape. Thus,  $\text{Var}(X_n)$  is independent of any

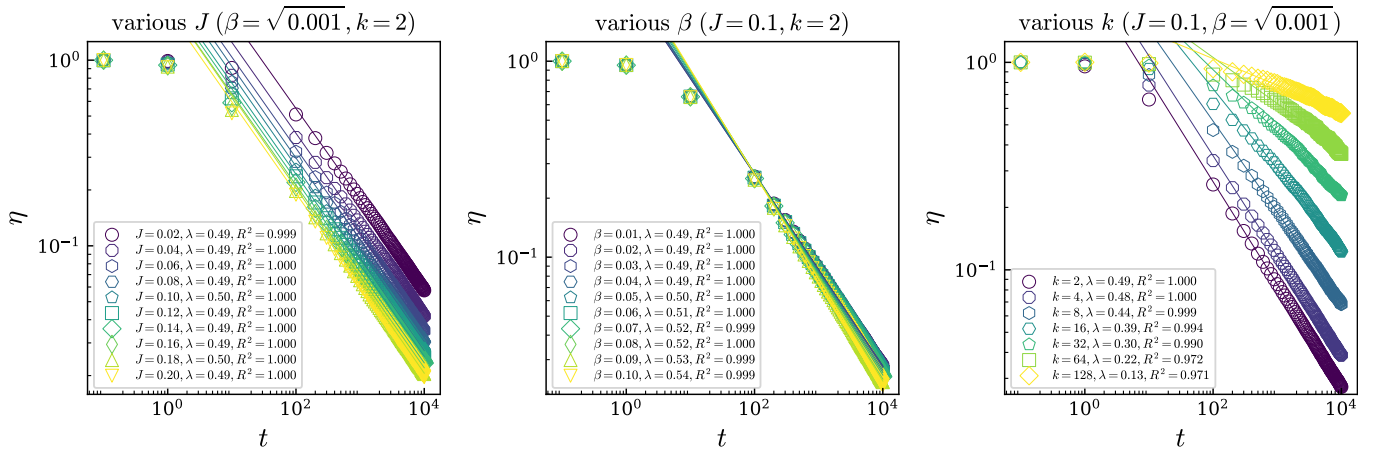


FIG. S2. The field exponent  $\eta(t)$  for various  $J, \beta, k$  conditions. The left panel is for various  $J$  with sufficiently small  $\beta = \sqrt{0.001}$ , the center panel is for various  $\beta$ , the right panel is for various  $k$  where  $k$  is number of neighbors in regular network of circular topology. All hollow dots represent numerical simulation results and solid lines represent least square linear regression for data samples with  $t > 10^2$ .  $R^2$  represent coefficient of determination for regression lines. For all cases, we used  $N = 10^4$  and ensemble average of 128 runs.

homogeneous deterministic drift term. This is the reason why we employ  $X_n = \ln c_n + \beta^2 t/2$  in Eq. (S2). Since the normalized wealth is defined as  $c \equiv C/\bar{C}$ , it should satisfy  $\langle c \rangle = 1$ . In addition,  $X$  follows the log-normal distribution with the mean  $\exp(\mu_t + \sigma_t^2/2)$ , where the corresponding drift is  $\mu_t = -\sigma_t^2/2$  as we mentioned in the main text. Therefore, the drift of  $x$  originates from the normalization drift that  $c$  is rescaled every step.

### B. Long-range correlation analysis

The  $\text{Cov}(X_n, \bar{X}_n)$  we obtained earlier is the log-scale wealth-wealth correlation between neighboring agents. We can go further and consider correlations between agents located at greater distances. For any agent  $n$ , let  $\bar{X}_{(n,\ell)}$  be the average wealth of agents of distance  $\ell$ , then  $\bar{X}_{(n,\ell)} = (X_{n-\ell} + X_{n+\ell})/2$ . Using the same process in SM-S1, we get

$$\frac{d}{dt} \text{Cov}(X_n, \bar{X}_{(n,\ell)}) = \beta^2 e^{-2Jt} I_\ell(2Jt). \quad (\text{S26})$$

The function  $e^{-2Jt} I_\ell(2Jt)$  on the right-hand side has a leading order of  $(2Jt)^\ell$  for small  $t$ . The  $X_n, X_{n+\ell}$  correlation between agents separated by a distance  $\ell$  is as following:

$$\text{Corr}(X_n, X_{n+\ell}) = \frac{\text{Cov}(X_n, X_{n+\ell})}{\sqrt{\text{Var}(X_n)\text{Var}(X_{n+\ell})}} = \frac{\text{Cov}(X_n, \bar{X}_{(n,\ell)})}{\text{Var}(X_n)}. \quad (\text{S27})$$

Note that  $\text{Var}(X_n) = \text{Var}(X_{n+\ell})$  by the translational invariance and be careful for  $\text{Cov}(X_n, X_{n+\ell}) = \text{Cov}(X_n, \bar{X}_{(n,\ell)})$  but  $\text{Corr}(X_n, X_{n+\ell}) \neq \text{Corr}(X_n, \bar{X}_{(n,\ell)})$ . For small  $t$ ,  $\text{Cov}(X_n, \bar{X}_{(n,\ell)}) \sim t^{\ell+1}$  and a leading term of  $\text{Var}(X_n) \sim t$ , so the correlation is

$$\text{Corr}(X_n, X_{n+\ell}) \sim t^\ell, \quad \text{for } t \ll 1. \quad (\text{S28})$$

Since initial condition  $c_n(0) = 1$ , first-order approximation is valid for small  $t$ . Thus,  $\text{Corr}(c_n, c_{n+\ell}) \simeq \text{Corr}(1 + x_n, 1 + \bar{x}_{(n,\ell)}) = \text{Corr}(x_n, \bar{x}_{(n,\ell)})$ . Therefore, we get

$$\text{Corr}(c_n, c_{n+\ell}) \sim t^\ell, \quad \text{for } t \ll 1. \quad (\text{S29})$$

This result theoretically supports the early-time correlation analysis by Medo [31]. We can also express  $\text{Corr}(X_n, X_{n+\ell})$  for large  $t$ .

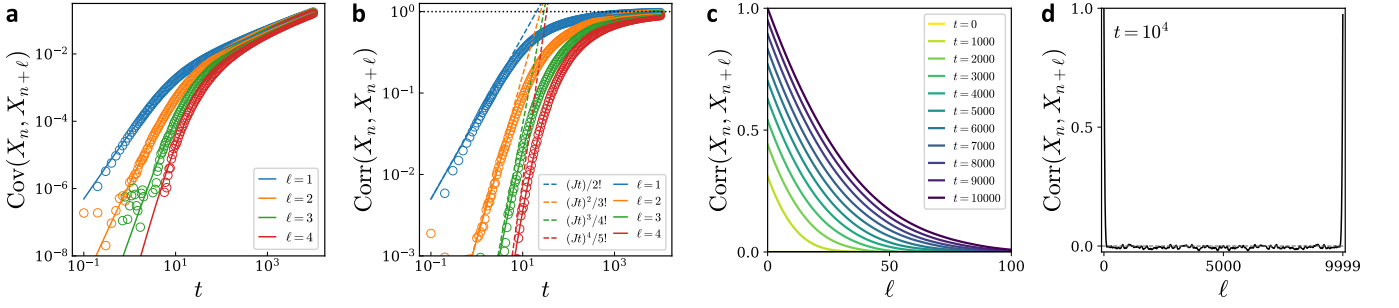


FIG. S3.  $\text{Cov}(X_n, X_{n+\ell})$  and  $\text{Corr}(X_n, X_{n+\ell})$  function of  $t$  for  $\ell = 1, 2, 3, 4$ . For (a) and (b), the hollow dots are numerical simulation results, solid lines are theoretical predictions, and dashed lines are leading order of the Taylor expansion of Eq. (S34) at  $t = 0$ ;  $\text{Corr}(X_n, X_{n+\ell})$  function of  $\ell$  for  $\ell \in [0, 100]$  and  $\ell \in [0, 9999]$ . For (c) and (d), the solid lines are numerical simulation results. For all cases,  $N = 10^4$ ,  $\alpha = 10^{-2}$ ,  $\Delta\alpha = 10^{-3}$ ,  $\beta^2 = 10^{-3}$ ,  $J = 10^{-1}$  and results are average of 128 ensembles.

Equation (S2) can be rewritten as multi-dimensional OU process as follows:

$$d\mathbf{X}_t = \mathbb{K}\mathbf{X}_t dt + \beta d\mathbf{W}_t, \quad (\text{S30})$$

where  $\mathbf{X}_t = (X_0, \dots, X_{N-1})$ ,  $\mathbf{W}_t = (W_{t,0}, \dots, W_{t,N-1})$  and  $\mathbb{K}$  is  $N \times N$  stability matrix given by

$$\mathbb{K} = J \begin{bmatrix} -1 & 1/2 & 0 & \dots & 1/2 \\ 1/2 & -1 & 1/2 & \dots & 0 \\ 0 & 1/2 & -1 & \dots & 0 \\ \vdots & \vdots & \vdots & \ddots & \vdots \\ 1/2 & 0 & 0 & \dots & -1 \end{bmatrix} \quad (\text{S31})$$

The stability of the system is determined by eigenvalues of  $\mathbb{K}$ . There are three cases: (1) stable case,  $\text{Re}(\lambda_n) < 0$  for all  $n$ , (2) marginally stable case,  $\text{Re}(\lambda_n) \leq 0$  and at least one  $\lambda_n = 0$ , (3) unstable case,  $\text{Re}(\lambda_n) > 0$  for at least one  $n$ . Since  $\mathbb{K}$  is circulant matrix, eigenvalues are

$$\lambda_n = -J \left( 1 - \cos \frac{2\pi n}{N} \right) \leq 0 \quad (n = 0, 1, \dots, N-1). \quad (\text{S32})$$

Thus,  $\mathbb{K}$  is marginally stable [40]. For this case, the system shows strongly auto-correlated behaviors for long-time scales. The  $\ell$ -ranged covariance can be obtained by definite integral of Eq. (S26). Let  $Q_\ell = \beta^2 \int_0^t e^{-2Js} I_\ell(2Js) ds$ . Then, covariance matrix  $\Sigma_t$  is

$$\Sigma_t = \beta^2 \begin{bmatrix} Q_0 & Q_1 & \dots & Q_{N/2-1} & Q_{N/2} & Q_{N/2+1} & \dots & Q_1 \\ Q_1 & Q_0 & \dots & Q_{N/2-2} & Q_{N/2-1} & Q_{N/2} & \dots & Q_2 \\ \vdots & \vdots & \ddots & \vdots & \vdots & \vdots & \ddots & \vdots \\ Q_1 & Q_2 & \dots & Q_{N/2} & Q_{N/2-1} & Q_{N/2-2} & \dots & Q_0 \end{bmatrix} \quad (\text{S33})$$

where the above expression for  $N$  is even. For the same time  $t$ , we check that  $\text{Cov}(X_n, X_{n+\ell})$  decreases over  $\ell$ . Here are some analytical expressions of covariance for  $\ell = 1, 2, 3, 4$ .

$$\text{Cov}(X_n, X_{n+\ell}) = \begin{cases} \frac{\beta^2}{2J} [-1 + (1 + 2Jt)e^{-2Jt} I_0(2Jt) + 2Jte^{-2Jt} I_1(2Jt)] & (\ell = 1) \\ \frac{\beta^2}{2J} [-2 + (2 + 2Jt)e^{-2Jt} [I_0(2Jt) + I_1(2Jt)]] & (\ell = 2) \\ \frac{\beta^2}{2J} \frac{1}{2Jt} [-3(2Jt) + 2Jt(5 + 2Jt)e^{-2Jt} I_0(2Jt) + [-4 + 2Jt(4 + 2Jt)]e^{-2Jt} I_1(2Jt)] & (\ell = 3) \\ \frac{\beta^2}{2J} \frac{1}{(2Jt)^2} [-4(2Jt)^2 + 16e^{-2Jt} I_1(2Jt) + 2Jt[-8 + 2Jt(8 + 2Jt)]e^{-2Jt} [I_0(2Jt) + I_1(2Jt)]] & (\ell = 4) \end{cases} \quad (\text{S34})$$

The corresponding  $\text{Corr}(X_n, X_{n+\ell})$  by Eq. (S34) have the leading order as  $\sim (Jt)^\ell / (\ell + 1)!$  for early time. And Eq. (S34) matches for large  $t$ . We also investigate the larger distance  $\ell$ . The smaller  $\ell$ , the larger  $\text{Corr}(X_n, X_{n+\ell})$ . The correlation vanishes for sufficiently large  $\ell$ . It implies that the system has a finite correlation length scale.

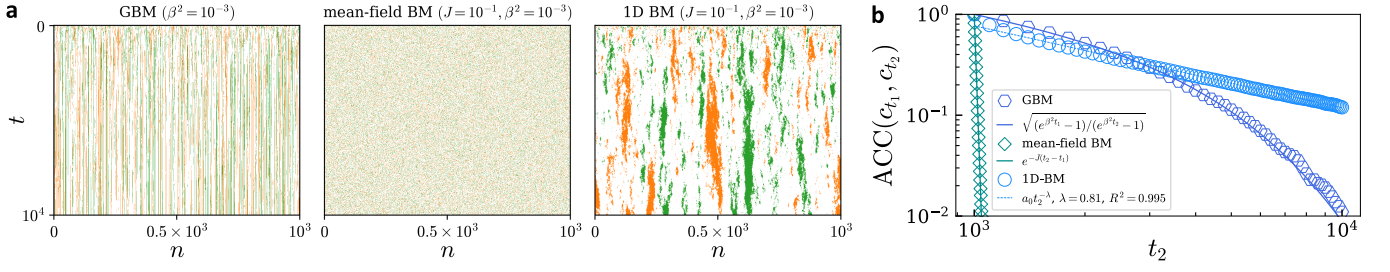


FIG. S4. (a) class dynamics of homogeneous ability models: geometric Brownian motion (GBM), mean-field BM model, and 1D BM model. The orange and green dots show top 10% and bottom 10% agents. (b) ACC for three models. The hollow dots are numerical simulation results, solid lines are theoretical predictions and dashed line is regression line. For all cases,  $N = 10^4$ ,  $\alpha = 10^{-2}$ ,  $\Delta\alpha = 10^{-3}$ ,  $\beta^2 = 10^{-3}$ .

### C. Autocorrelation coefficient (ACC) for various network topologies

In the main text, we mention that the geometric Brownian motion (GBM) and the mean-field BM model show the exponential decay of the ACC. This means that the relative wealth of agents does not persist for long time. We define the ACC [60] as follows:

$$\text{ACC}(c_{t_1}, c_{t_2}) \equiv \frac{\text{Cov}(c_{t_1}, c_{t_2})}{\sqrt{\text{Var}(c_{t_1})\text{Var}(c_{t_2})}}. \quad (\text{S35})$$

For the GBM by  $C_t = C_0 \exp[(\alpha - \beta^2/2)t + \beta W_t]$  and  $\mathbb{E}[e^{X+Y}] = \exp[\mu_X + \mu_Y + (\mu_X^2 + \mu_Y^2)/2 + \text{Cov}(X, Y)]$  dependent Gaussian random variable  $X, Y$ , we get the following statistics: (1)  $\text{Var}(c_t) = e^{2\alpha t}(e^{\beta^2 t} - 1)$ , and (2)  $\text{Cov}(c_t, c_s) = e^{\alpha(t+s)} [e^{\beta^2 \min(t,s)} - 1]$ . Thus,  $\text{ACC}(c_t, c_s) = \sqrt{(e^{\beta^2 s} - 1)/(e^{\beta^2 t} - 1)}$  where  $t > s$  and  $\text{ACC}(c_t, c_s) \approx e^{-\beta^2 |t-s|/2}$  for large  $(t, s)$ . For the mean-field BM model, the ACC is known as  $e^{-J\Delta t}$  [25] for the condition of  $2J/\beta^2 > 1$ . In contrast to the ACC decays exponentially for a non-interacting case and an extremely dense network, for the 1D ring topology, the ACC follows time-asymptotic power-law behavior  $\text{ACC} \sim \Delta t^{-\xi}$  for the large time different  $\Delta t = t_2 - t_1$  and  $c_t$  of them follow the long-memory process [61] since  $0 < \xi < 1$  [see Fig. S4-(b)].

## II. STATISTICAL PROPERTIES OF BINARY MIXTURE FOR 1D RING TOPOLOGY

In this section, we check the statistical properties of binary mixtures for the ring topology.

### A. Assortativity $\mathcal{A}$

First, an ability assortativity is defined as  $\mathcal{A} \equiv \text{Cov}(\alpha, \alpha')/\sqrt{\text{Var}(\alpha)\text{Var}(\alpha')}$  where  $\alpha$  and  $\alpha'$  are the abilities of neighboring agents and  $\alpha \in \{\alpha_0 - \Delta\alpha, \alpha_0 + \Delta\alpha\}$ . If we let  $N_+$  ( $N_-$ ) as the number of agents with lower (higher) ability, we simply find that  $\text{Var}(\alpha) = \text{Var}(\alpha') = \frac{1}{N} [\frac{N}{2}(\alpha_0 - \Delta\alpha)^2 + \frac{N}{2}(\alpha_0 + \Delta\alpha)^2] - \alpha_0^2 = \Delta\alpha^2$ . For a ring topology, the number of links is the same as the number of nodes  $N$ . The number of nodes can be decomposed by  $N = N_{ll} + N_{hh} + N_{lh}$ , where  $N_{ll}$  ( $N_{hh}$ ) is the number of links between lower (higher)  $\alpha$  nodes and  $N_{lh}$  is the number of links between  $\alpha_-$  and  $\alpha_+$  nodes. For this case,

$$\begin{aligned} \text{Cov}(\alpha, \alpha') &= \frac{1}{N} [N_{ll}(\alpha_0 - \Delta\alpha)^2 + N_{hh}(\alpha_0 + \Delta\alpha)^2 + N_{lh}(\alpha_0 - \Delta\alpha)(\alpha_0 + \Delta\alpha)] - \alpha_0^2 \\ &= \frac{N_{ll} + N_{hh} + N_{lh}}{N} \Delta\alpha^2 + (N_{hh} - N_{ll})(2\alpha_0\Delta\alpha) = \frac{N^{(\text{ho})} - N^{(\text{he})}}{N} \Delta\alpha^2. \end{aligned} \quad (\text{S36})$$

To reflect changes in link configuration for each pair node swapping, we must consider two neighboring  $\alpha$  of selected node. Each node can be categorized by 3-consecutive network motifs. For this case, there are 6 motifs and possible cases of center node swapping between motifs are  $\binom{6}{2}$ . For all possible cases,  $\Delta N_{ll} = \Delta N_{hh}$ , thus,  $N_{ll} - N_{hh}$  is conserved under any pair node swapping. Therefore, for the case of  $N_- = N_+$ ,  $N_{ll} = N_{hh}$ . If we let homogeneous

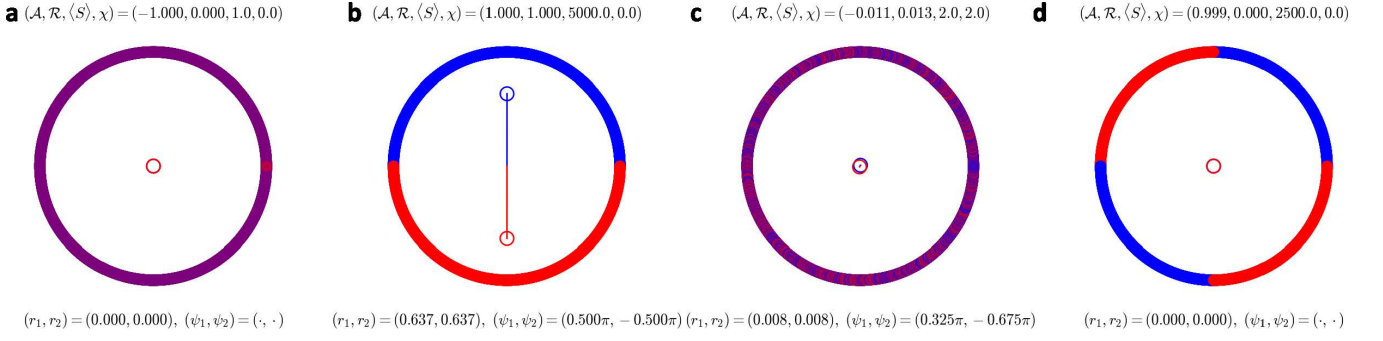


FIG. S5. Statistics  $(\mathcal{A}, \mathcal{R}, \langle S \rangle, \chi)$  and order parameters  $(r, \psi)$  of binary mixture for 1D ring topology. (a) Perfectly disassortative configuration; (b) Perfectly assortative configuration; (c) Randomly permuted configuration, and (d) regularly clustered configuration for  $\langle S \rangle = 2500$ . For all cases,  $N = 10^4$  and  $N_1 = N_2 = 5 \times 10^3$ .

and heterogeneous link density as  $\rho^{(1)} = (N_{ll} + N_{hh})/N$  and  $\rho^{(2)} = N_{lh}/N$ , we finally find that  $\mathcal{A} = \rho^{(1)} - \rho^{(2)}$  for  $N_+ = N_-$ .

### B. Kuramoto oscillators' phase order parameters $(r, \psi)$

We only consider  $N_+ = N_-$  where the numbers of each binary element are the same. For perfectly assortative configuration  $(\mathcal{A}_{\max})$  in large  $N$ , we can calculate  $(r_1, \psi_1), (r_2, \psi_2)$  as follows:

$$r_+ e^{i\psi_+} = \frac{1}{N/2} \sum_{j=1}^{N/2} e^{i(2\pi j/N)} = \frac{1}{2\pi} \frac{2\pi}{N/2} \sum_{j=1}^{N/2} e^{i(2\pi j/N)} \rightarrow \frac{1}{\pi} \int_0^\pi e^{iu} du = \frac{2}{\pi} i. \quad (\text{S37})$$

$$r_- e^{i\psi_-} = \frac{1}{N/2} \sum_{j=N/2+1}^N e^{i(2\pi j/N)} = \frac{1}{2\pi} \frac{2\pi}{N/2} \sum_{j=N/2+1}^N e^{i(2\pi j/N)} \rightarrow \frac{1}{\pi} \int_\pi^{2\pi} e^{iu} du = -\frac{2}{\pi} i. \quad (\text{S38})$$

As a result, we get order parameters as  $(r_+, \psi_+) = (\frac{2}{\pi}, \frac{\pi}{2}), (r_-, \psi_-) = (\frac{2}{\pi}, \frac{3\pi}{2})$ , where  $2/\pi$  is the maximum value of  $r$ . For arbitrary configuration only except the case of  $r \neq 0$ , the following relations are satisfied:

$$r_+ = r_- = r, \quad \Delta\psi = |\psi_+ - \psi_-| = \pi. \quad (\text{S39})$$

The whole configurations can be obtained by pair node swapping starting from perfectly assortative configuration. Thus, if above relations (S39) are robust under the arbitrary pair-node swapping, we can say that they are the universal properties for the binary mixture of the ring topology.

Consider an initial binary configuration, the order parameters are  $\vec{r}_+, \vec{r}_-$ , where these are represented by the real vector form. We assume that the initial configuration satisfies  $\vec{r}_+ = -\vec{r}_-$ . When arbitrary nodes  $(j, k)$  are swapped, there are two cases: (1)  $(j, k)$  belong to the same binary element group, (2)  $(j, k)$  are in the different binary element groups. For the first case, the order parameters do not change. For the second case, the order parameters of swapped configuration are as follows:

$$\vec{r}'_+ = \vec{r}_+ - \vec{a}_j + \vec{a}_k = \vec{r}_+ + \vec{A}. \quad (\text{S40})$$

$$\vec{r}'_- = \vec{r}_- + \vec{a}_j - \vec{a}_k = \vec{r}_- - \vec{A}, \quad (\text{S41})$$

where  $\vec{a}_j = (\cos \frac{2\pi j}{N}, \sin \frac{2\pi j}{N})$  and  $\vec{A} = \vec{a}_k - \vec{a}_j$ . Since  $\vec{r}_+ = -\vec{r}_-$ ,  $\vec{r}'_- = \vec{r}_- - \vec{A} = -(\vec{r}_+ + \vec{A}) = -\vec{r}'_+$ . Thus,  $\vec{r}'_-$  has the same length and the opposite direction, compared to  $\vec{r}'_+$ . Therefore, Eq. (S39) is satisfied under the arbitrary pair node swapping only except the cases of  $\vec{r}'_1 = 0$  or  $\vec{r}'_2 = 0$ . For an instance, *path 1, 2*, in the main text (see Fig. 1) satisfies above properties only except for the perfectly disassortative configuration  $(\mathcal{A}_{\min}, \mathcal{R}_{\min})$ . There are several cases that satisfies  $r = 0$ , excluding the perfectly disassortative configuration. If the same binary elements are allocated in the exactly opposite direction for all locations,  $r = 0$ . For this case, an angular argument  $\psi$  cannot be defined.

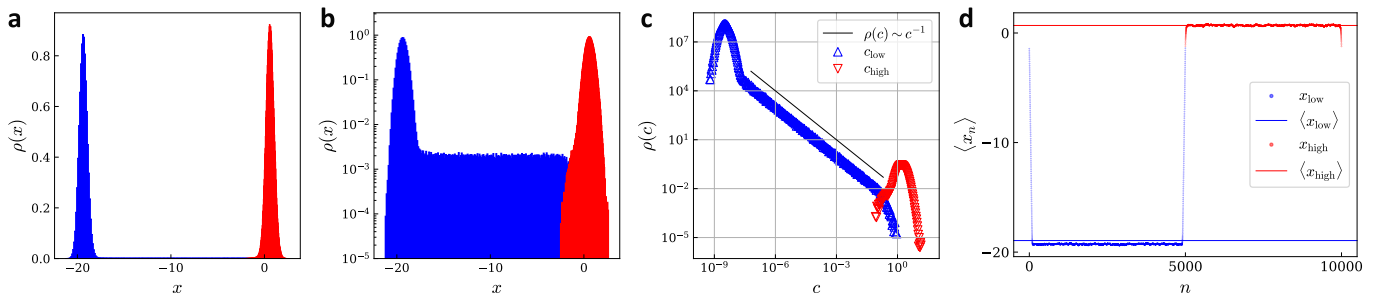


FIG. S6. The distributional properties for  $\mathcal{A}_{\max}$  case. (a)  $\rho_{\alpha-\Delta\alpha}(x)$  (blue),  $\rho_{\alpha+\Delta\alpha}(x)$  (red). (b)  $\rho(x)$  as log-scale. (c) Corresponding  $\rho(c)$  for double logarithmic scale. The black solid line shows trend line for  $\rho(c) \sim c^{-1}$ . (d) The positional average of  $x$ :  $\langle x_n \rangle$ . For all cases,  $N = 10^4$ ,  $\alpha = 10^{-2}$ ,  $\Delta\alpha = 10^{-3}$ ,  $\beta^2 = 10^{-3}$ ,  $J = 10^{-1}$  and results are average of 128 ensembles. The given snapshots are at  $t = 10^4$

### C. Cluster size distribution $P(S)$

The other significant statistics are the average cluster size  $\langle S \rangle$  and the cluster size variance  $\chi$ . For  $N_+ = N_-$  and  $N \rightarrow \infty$ , the binary mixture in a ring can be considered as the random sequence of a binary element with the same probability  $p = 1/2$ . If we define cluster as consecutive sequence of same binary element, the probability mass function of cluster size  $P(S)$  is geometric:

$$P(S) = \frac{1}{2^{S+1}}. \quad (\text{S42})$$

The expected cluster size is  $\langle S \rangle = \mathbb{E}[S] = \sum_{S=1}^{\infty} S \cdot P(S) = 2$ . Moreover, the expected cluster size variance is  $\chi = \mathbb{E}[S^2] - \mathbb{E}[S]^2 = 2$ . Thus, the randomly permuted binary mixture gives  $(\langle S \rangle, \chi) = (2, 2)$  for  $N \rightarrow \infty$ . In particular, if all the cluster sizes are the same, this configuration satisfies  $\chi = 0$ ,  $N/(2\langle S \rangle) \in \mathbb{N}$ , and  $\mathcal{R} = 0$ . For these regularly clustered configurations, the different cluster size  $\langle S \rangle$  (or assortativity  $\mathcal{A}$ ) affects the system dynamics.

## III. HETEROGENOUS BOUCHAUD-MÉZARD (HBM) MODEL FOR 1D RING TOPOLOGY

### A. Normalized wealth distribution for perfectly assortative ability configuration

Let  $\rho(x)$ ,  $\rho_{\alpha-}(x)$ ,  $\rho_{\alpha+}(x)$  as the probability density function of  $x$  in the entire lower and higher ability groups. For a perfectly disassortative ability configuration,  $\mathcal{A}_{\min}$ ,  $\rho_{\alpha-\Delta\alpha}(x)$  and  $\rho_{\alpha+\Delta\alpha}(x)$  almost perfectly overlapped, and the overall distribution is almost the same as that in the ordinary BM model. Therefore,  $\rho(c, t; \mathcal{A}_{\min}) \sim \text{Lognormal}(\mu_t, \sigma_t^2)$ .

For a perfectly assortative ability configuration,  $\mathcal{A}_{\max}$ , the situation is more complicated. For this case,  $\rho(x, t)$  is not unimodal. The distribution can be roughly divided into three parts: (1) a peak around the first mode (head), (2) between the two peaks (intermediate/body), and (3) near the second peak (tail). To see more precisely how many samples exist between the two peaks, we plot the y-axis in a logarithmic scale, and surprisingly, we find that the  $x$  samples between the two peaks follow a uniform distribution, with most of them belonging to the  $\alpha_-$  group. For  $\mathcal{A}_{\max}$ ,  $\rho_{\alpha-\Delta\alpha}(x)$  and  $\rho_{\alpha+\Delta\alpha}(x)$  are asymmetric over  $x$ , whereas, for  $\mathcal{A}_{\min}$ , they are symmetric. The double logarithmic scaled plot shows the intermediate region, where the power-law decay of  $\rho(c) \sim Ac^{-1}$  with a constant  $A$ . This is a natural consequence of the distribution transformation formula,  $\rho(c) = \rho(x)|dx/dc| = A|d(\ln c)/dc| = Ac^{-1}$ . Our main hypothesis to explain the regional separation of the distribution function is that a field exponent  $\eta$  is a function of the agent's position  $n$  in the network.

In the main text, we obtain Eq.(8) via the first-order approximation, assuming that  $\eta x$  is sufficiently small. However, if  $\eta$  is extremely small, interaction term  $J[\theta(\eta)c^{1-\eta} - c]dt$  can be neglected since  $c^{1-\eta} \rightarrow c$  and  $\theta(\eta) \rightarrow 1$ . Therefore, equation can be separated as the following two cases:

$$dc_n = J[\theta(\eta)c_n^{1-\eta} - c_n]dt + \beta c_n dW_{t,n} \rightarrow \begin{cases} dx_n & = J\eta_{t,n}[\mu_{t,n} - x_n]dt + \beta dW_{t,n}. \\ dc_n & = \beta c_n dW_{t,n}. \end{cases} \quad (\text{S43})$$

If our hypothesis is correct, the governing equation for  $\rho(c, t)$  should depend on the agent's position  $n$  in the network.

To check this, we plot the average of  $x_n$  for a given position  $n$ , i.e.,  $\langle x_n \rangle$ , and the result is shown in Fig. S6. In the intermediate region between two different ability clusters,  $\langle x_n \rangle$  are almost equidistantly spaced proportional to  $n$ . Also, since  $\langle x_n \rangle$  is the ensemble average at position  $n$ , implying that there are the same number of agent samples corresponding to each value. Therefore,  $x$  drawn from these samples of agents will be uniformly distributed over the entire  $\rho(x)$ . Since the number of samples is the same at each point,  $\rho^{(b)}(x, t) = \text{const}$  and therefore,  $\frac{\partial}{\partial t}\rho^{(b)}(c, t) = 0$ . The Fokker-Planck equation for the second case of Eq. (S43) is

$$\frac{\partial}{\partial t}\rho(c, t) = \frac{1}{2} \frac{\partial^2}{\partial c^2} [\beta^2 c^2 \rho(c, t)]. \quad (\text{S44})$$

For the intermediate region, since  $\frac{\partial}{\partial t}\rho^{(b)}(c, t) = 0$ , the solution is  $\rho^{(b)}(c, t) = Ac^{-1} + Bc^{-2}$ , where  $A$  and  $B$  are constants. Our observation from numerical simulations is  $\rho^{(b)}(c, t) \sim Ac^{-1}$ , which supports  $B = 0$ . Thus, the governing equation for  $c_n$  in this region is equal to the second case of Eq. (S43). So we can expect that  $\eta$  measured from these samples is extremely small. For this case, we call the set of agents the intermediate class if the wealth distribution follows power-law as  $\rho(c) \sim Ac^{-1}$ . Automatically, the regions excluding the intermediate class should be the head class, represented by small  $\langle x_n \rangle$ , and the tail class, represented by large  $\langle x_n \rangle$ , respectively.

The question is how to determine the position set of the intermediate class. We considered this range as the interval where the  $c$  follows power-law, but despite its simplicity, this definition is impractical from a point of view of numerical simulation: it is almost impossible to explore all possible combinations of position sets for all  $c$  samples at every time. Therefore, we use the standard deviation maximization (SDM) method as a simple technique to classify the intermediate class. For the intermediate region, the values of  $\langle x_n \rangle$  are approximately equidistantly spaced proportional to  $n$ , so  $x \sim \text{Uniform}(a, a + [n_f - n_i]\Delta x)$ . We start from the contact point of  $\alpha_0 - \Delta\alpha$  and  $\alpha_0 + \Delta\alpha$ , and sequentially collect a sample of nodes within distance  $d_1$  ( $d_2$ ) in the direction of the  $\alpha_{\pm}$  cluster. We stop further investigation at  $d_1$  and  $d_2$ , where the standard deviation of  $x$  is maximized, and consider the agents falling into this region to be the intermediate class. Although the  $x$  distribution of the intermediate class classified by this method is U-shaped rather than a complete uniform distribution, most of the  $x$  values lie in the uniform distribution region, and the remaining regions are the lower and upper classes. We confirm by skewness and kurtosis tests that the  $x_n$  distribution is almost Gaussian for head and tail regions. Therefore, by using the SDM method, we can simply classify the node samples corresponding to two Gaussian peaks and one uniform distribution.

Figure S7 (e) shows the  $\eta(t)$  for each region: the head and tail classes show the power-law decays same as the BM model, while  $\eta$  for the intermediate class decreases much faster. Specifically, at  $t = 10^4$ , the order of  $\eta$  is smaller than  $10^{-4}$ , so the interaction term in Eq. (S43) can be neglected. Therefore, dynamics of head and tail class are governed by first case of equation and follows log-normal distribution, also, intermediate class samples are governed by second cases of equation and follows a power-law distribution. The remainders are drift  $\mu_{t,n}$  for head and tail classes. To figure it out, we first consider the null model, where the two ability groups are completely separated by two 1D rings. Thus, there is no intermediate region. For this case, each group follows the independent BM model, and the underlying equation is the same as Eq.(2) in the main text. The average wealth of them are  $\langle C_{\text{low}}(t) \rangle = C(0)e^{(\alpha_0 - \Delta\alpha)t}$  and  $\langle C_{\text{high}}(t) \rangle = C(0)e^{(\alpha_0 + \Delta\alpha)t}$ . Then, the corresponding average normalized wealth for each group is:

$$\langle c_{\text{low}} \rangle_{\text{null}} = \frac{C(0)e^{(\alpha_0 - \Delta\alpha)t}}{[C(0)e^{(\alpha_0 - \Delta\alpha)t} + C(0)e^{(\alpha_0 + \Delta\alpha)t}]/2} = \frac{2}{1 + e^{2\Delta\alpha t}}. \quad (\text{S45})$$

$$\langle c_{\text{high}} \rangle_{\text{null}} = \frac{C(0)e^{(\alpha_0 + \Delta\alpha)t}}{[C(0)e^{(\alpha_0 - \Delta\alpha)t} + C(0)e^{(\alpha_0 + \Delta\alpha)t}]/2} = \frac{2}{1 + e^{-2\Delta\alpha t}}. \quad (\text{S46})$$

Since each group follows a log-normal distribution, and the variance is  $\sigma_t^2 = \beta^2 t^\lambda / (2Ja_0)$  for large  $t$  as in the BM model, the normalization conditions for them are:  $\langle c_{t,\text{low}} \rangle = \exp(\mu_{t,\text{low}} + \sigma_t^2/2)$  and  $\langle c_{t,\text{high}} \rangle = \exp(\mu_{t,\text{high}} + \sigma_t^2/2)$  where  $\mu_{t,\text{low}} = \langle x_{\text{low}} \rangle$  and  $\mu_{t,\text{high}} = \langle x_{\text{high}} \rangle$ . Therefore,

$$\langle x_{\text{low}} \rangle_{\text{null}} = -\frac{\beta^2}{4Ja_0} t^\lambda + \ln\left(\frac{2}{1 + e^{2\Delta\alpha t}}\right). \quad (\text{S47})$$

$$\langle x_{\text{high}} \rangle_{\text{null}} = -\frac{\beta^2}{4Ja_0} t^\lambda + \ln\left(\frac{2}{1 + e^{-2\Delta\alpha t}}\right). \quad (\text{S48})$$

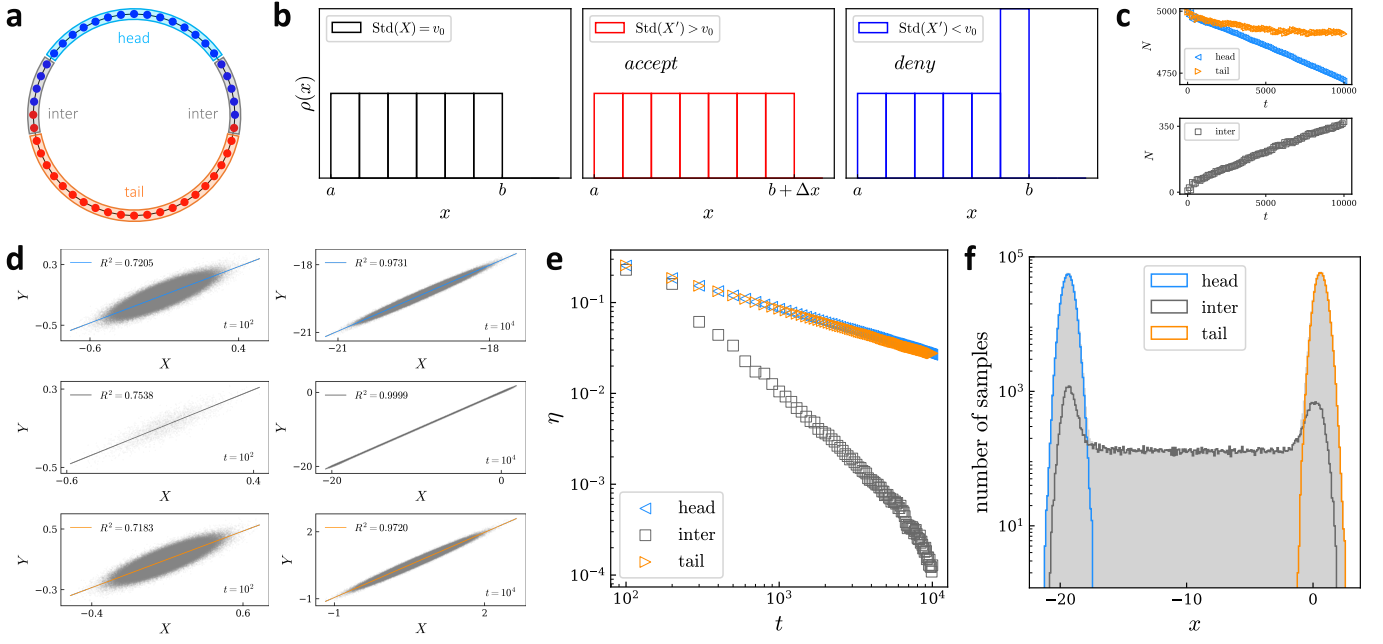


FIG. S7. Positional separation for  $\mathcal{A}_{\max}$  case. (a) Conceptual visualization for separation of governing equation on 1D ring. The field exponent  $\eta$  separated by three regions: head, intermediate, and tail. (b) Standard deviation maximization (SDM) algorithm. To detect intermediate region, We start from active node (the agent who has heterogeneous link) and select set of nodes within the range  $[d_1, d_2]$  from active node. After that, investigate standard deviation of  $X$  from these node samples and find the range  $[d_1, d_2]$  which maximize  $\text{Std}(X)$ . (c) Size evolution of each regions. (d) Correlation between  $X = \ln c$  and  $Y = \ln \bar{c}_n$  for each region at  $t = 10^2$  and  $t = 10^4$ . (e)  $\eta(t)$  for head, intermediate, and tail regions. (f) Portion of  $x$  samples for head, intermediate, and tail regions. For all cases of (c), (d), (e), (f),  $N = 10^4$ ,  $\alpha = 10^{-2}$ ,  $\Delta\alpha = 10^{-3}$ ,  $\beta^2 = 10^{-3}$ ,  $J = 10^{-1}$ .

Approximately for large  $t$ ,

$$\langle x_{\text{high}} \rangle_{\text{null}} - \langle x_{\text{low}} \rangle_{\text{null}} \approx 2\Delta\alpha t, \quad (\text{S49})$$

which means interval between two Gaussian peaks linearly increases over time. Reflects the segregation of the wealth (or income) level between two  $\alpha$  groups, and the greater the deviation of the ability  $\Delta\alpha$  makes the segregation of the wealth level faster.

Figure S8 shows that in the HBM model for  $\mathcal{A}_{\max}$ , the average of  $x$  is the same as null model for head class but slightly different for the tail class. Thus,  $\langle x_{t,\text{head}} \rangle = \langle x_{t,\text{low}} \rangle_{\text{null}}$  but  $\langle x_{t,\text{tail}} \rangle \neq \langle x_{t,\text{high}} \rangle_{\text{null}}$ . It means that the head class classified by the SDM method has the same average normalized wealth but tail class is not. Thus, we additionally check the difference between the wealth-level segregation of the null model and the HBM model with  $\mathcal{A}_{\max}$ , and find that the difference increases roughly decreases over time:  $(\langle x_{\text{high}} \rangle - \langle x_{\text{low}} \rangle) - 2\Delta\alpha t \sim b_0 t$ . Earlier, we checked that most of the agents in the uniform distribution region belong to the  $\alpha_-$  group and only a small fraction belong to the  $\alpha_+$  group. As the distance between the two Gaussian peaks increases over time, the area of the uniform distribution in the intermediate region increases. However, since  $\rho(x, t) = \text{const}$  in this region, samples that belonged to the Gaussian region in are absorbed into the uniform distribution region over time. At this moment, the more samples in  $\alpha_-$  group absorbed into uniform region than in  $\alpha_+$  group. Therefore, the difference in the relative heights of the modes of the normal distributions grows as the uniform distribution region widens over time. Figure S7-(c) shows number of samples for each class. Finally, we summarize the results as follows:

$$\left\{ \mu_{t,\text{head}} = -\frac{\sigma_t^2}{2} + \ln\left(\frac{2}{1 + e^{2\Delta\alpha t}}\right), \quad \mu_{t,\text{tail}} = -\frac{\sigma_t^2}{2} + \ln\left(\frac{2}{1 + e^{-2\Delta\alpha t}}\right) + b_0 t, \quad \sigma_t^2 = \frac{\beta^2}{2Ja_0} t^\lambda \right\}. \quad (\text{S50})$$

$$\rho^{(\text{h})}(c, t) \sim \text{Lognormal}(\mu_{t,\text{head}}, \sigma_t^2), \quad \rho^{(\text{b})}(c, t) \sim Ac^{-1}, \quad \rho^{(\text{t})}(c, t) \sim \text{Lognormal}(\mu_{t,\text{tail}}, \sigma_t^2). \quad (\text{S51})$$

$$\mu_{t,\text{tail}} - \mu_{t,\text{head}} \approx (2\Delta\alpha - b_0)t \quad (\text{S52})$$

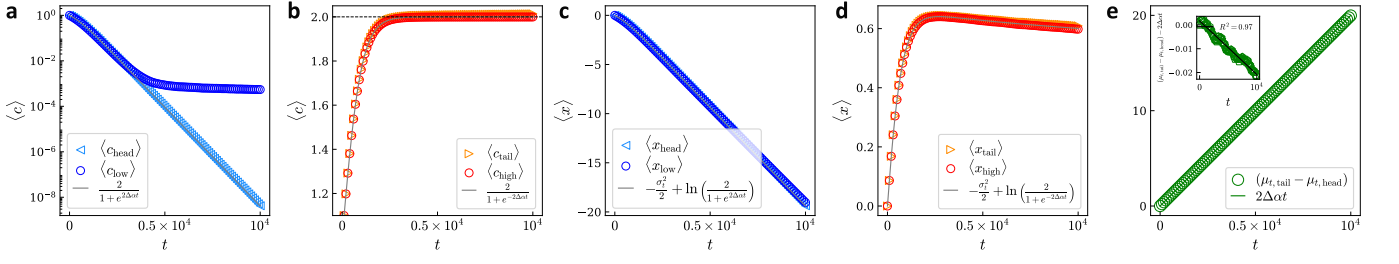


FIG. S8. Ensemble averages and wealth-level segregation for  $\mathcal{A}_{\max}$  case. (a), (b) Time evolutions of  $\langle c \rangle$  for head, lower, tail, and higher classes. (c), (d) Time evolutions of  $\langle x \rangle$  for head, lower, tail, and higher classes. (e) Interval between two Gaussian peaks (see Fig. S7-f) of head and tail classes which represent segregation of wealth-level. Inset in (e) shows difference between  $\langle x_{\text{high}} \rangle - \langle x_{\text{low}} \rangle$  and  $2\Delta\alpha t$ . For all cases,  $N = 10^4$ ,  $\alpha = 10^{-2}$ ,  $\Delta\alpha = 10^{-3}$ ,  $\beta^2 = 10^{-3}$ ,  $J = 10^{-1}$  and results are average of 128 ensembles.

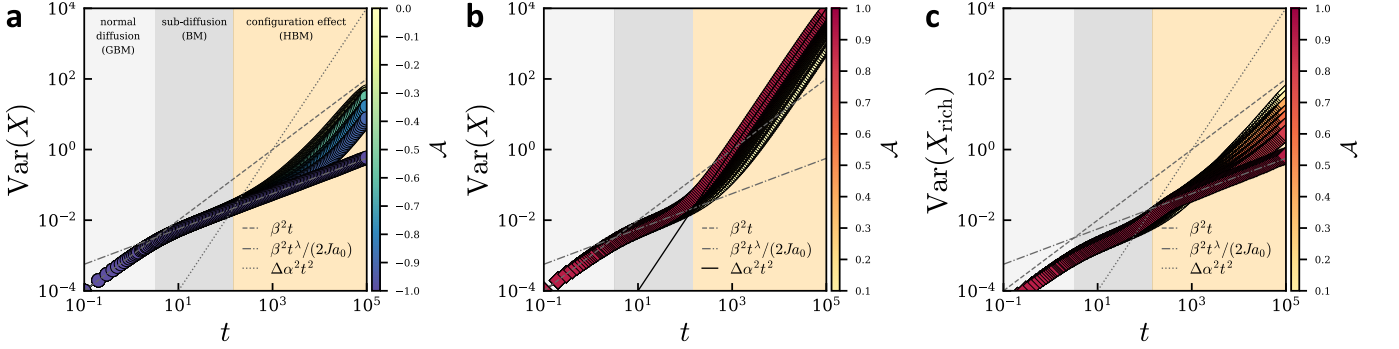


FIG. S9. Variances in the HBM model for various configurations. The ability configurations are chosen from random pair swapping path 1 and 2 (see Fig. 1-(d) in the main text). (a)  $\text{Var}(X)$  for only diffusion regime ( $\mathcal{R} \simeq 0, \mathcal{A} \leq 0$ ) (b), (c)  $\text{Var}(X)$ ,  $\text{Var}(X_{\text{rich}})$  for diffusion and segregation regime ( $\mathcal{R} > 0, \mathcal{A} > 0$ ).  $X_{\text{rich}}$  means  $X$  samples excess median  $X$ . For all cases,  $N = 10^4$ ,  $\alpha = 10^{-2}$ ,  $\Delta\alpha = 10^{-3}$ ,  $\beta^2 = 10^{-3}$ ,  $J = 10^{-1}$  and results are average of 128 ensembles.

where  $\Delta\alpha \gg b_0$ . It seems trivial that wealth-level segregation is determined by the difference of ability ( $\alpha$ ) between two groups. Eq. (S49) shows that it is true only if there is no heterogeneous (active) link in the  $\alpha$ -configuration. However, for the general cases, wealth-level does not perfectly divided by agent abilities because abilities are not perfectly concentrated on the 1D ring topology. Thus, for  $\mathcal{R} < 1$ , agent who has  $\alpha_-$  can be rich class and vice versa. Thus, the smaller  $\mathcal{R}$ , the smaller Hellinger distance. The correlation between  $\alpha$  and  $x$  also does (see Fig. 2 in the main text). Therefore, it is not trivially true that wealth-level segregation is determined by ability difference for the general case which heterogeneous agents are connected in the network.

## B. Diffusive nature and ballistic motion in the HBM model

In the HBM model for the 1D ring topology, total variance of  $X$  passes 3 phases: (1) Normal diffusion, (2) Sub-diffusion, and (3) Configuration effect dominant region and these are inherited from the GBM, the 1D BM model, and 1D HBM model, respectively. For  $\mathcal{A}_{\max}$ , we find that  $\text{Var}(X)$  increases very fast and is proportional to  $\sim t^2$  for large  $t$ . In this case,  $\rho(x, t)$  can be approximated by the dual Gaussian mixture of  $\mathcal{N}(\mu_1, \sigma_t^2), \mathcal{N}(\mu_2, \sigma_t^2)$  as in Eq. (S2). Thus,

$$\text{Var}(X; \mathcal{A}_{\max}) \approx \sigma_t^2 + \frac{(\mu_1 - \mu_2)^2}{4} = \frac{\beta^2}{2Ja_0} t^\lambda + \Delta\alpha^2 t^2, \quad (\text{S53})$$

where  $\mu_1 - \mu_2 \approx 2\Delta\alpha t$  as we checked in Eq. (S52). Since  $1/2 \leq \lambda < 1$ ,  $\text{Var}(X; \mathcal{A}_{\max}) \approx \Delta\alpha^2 t^2$  for large  $t$ . The others cases of  $\mathcal{R} > 0$  also undergo class division so that distance between probability density peaks linearly increases over time, which means  $\text{Var}(X)$  is dominated by not diffusion but ballistic motion (see Fig. S9-(b)). Due to both segregation and diffusion in the rich class affect  $g$ , we have investigated  $\text{Var}(X_{\text{rich}})$  separately.

The variances are shaped by triple time scales:  $\{\beta^2 t, \beta^2 t^\lambda / (2Ja_0), \Delta\alpha^2 t^2\}$ . By finding intersections of them, we can

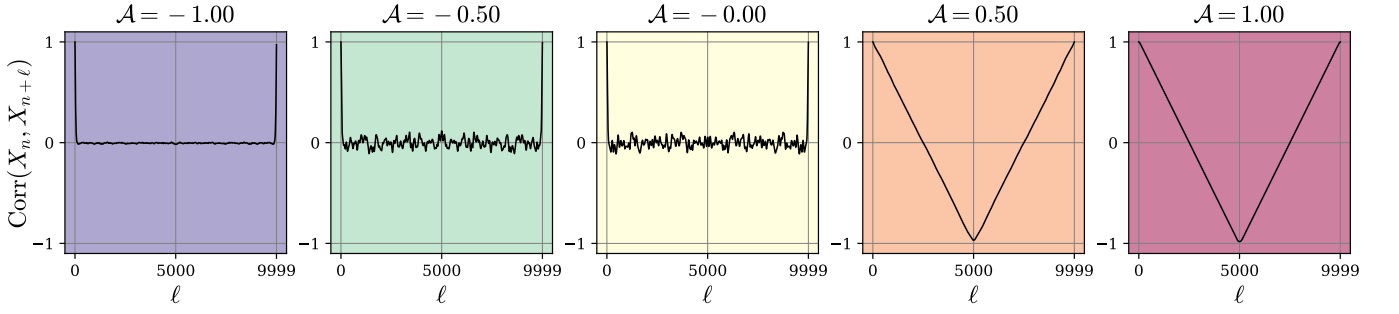


FIG. S10. Long-range correlations in the HBM model at  $t = 10^4$  for various  $\alpha$ -configurations. The ability configurations are chosen from random pair swapping path 1 and 2 (see Fig. 1 in the main text). For all cases,  $N = 10^4$ ,  $\alpha = 10^{-2}$ ,  $\Delta\alpha = 10^{-3}$ ,  $\beta^2 = 10^{-3}$ ,  $J = 10^{-1}$  and results are average of 128 ensembles.

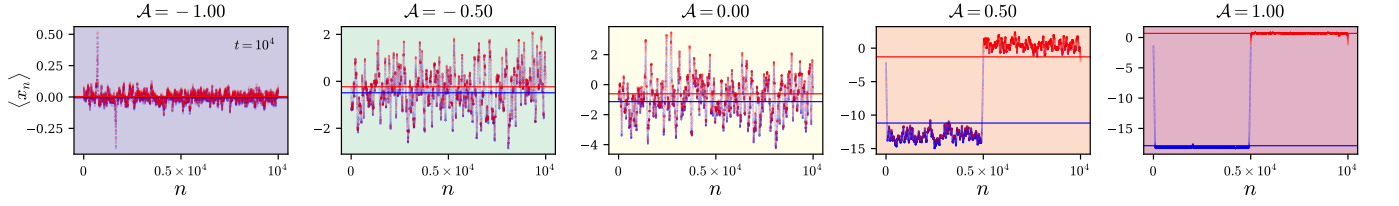


FIG. S11. Positional mean  $\langle x_n \rangle$  at  $t = 10^4$ , regional convergence and segregation of wealth-level. The ability configurations are chosen from random pair swapping path 1 and 2. Red and blue dots represent  $\langle x_n \rangle$  for lower and  $\alpha_+$  group. The red and blue horizontal solid lines show  $\langle x_{\alpha \pm \Delta\alpha} \rangle$ , respectively. For all cases,  $N = 10^4$ ,  $\alpha = 10^{-2}$ ,  $\Delta\alpha = 10^{-3}$ ,  $\beta^2 = 10^{-3}$ ,  $J = 10^{-1}$  and results are average of 128 ensembles.

determine the periods of each phase. The corresponding intersections are  $t_1 = (2Ja_0)^{\frac{1}{\lambda-1}}$  and  $t_2 = \left[ \frac{\beta^2}{2Ja_0\Delta\alpha^2} \right]^{\frac{1}{2-\lambda}}$ . For  $t > t_2$ , the system deviates from the sub-diffusive nature of 1D-BM model and enters the configuration-effect dominant phase in the HBM model. This is the unique feature of the HBM model since absence of configuration effect makes the BM model ends with the sub-diffusion. Also, from the analytical form of  $t_2$ , we can easily expect that the sub-diffusion phase will vanish if  $\Delta\alpha$  has much larger order than  $\beta$ .

### C. Spatial and long-range correlation analysis

As a measure for spatial correlation, global Moran's index I [62] usually used.

$$I = \frac{(1/W) \sum_{i=1}^N \sum_{j=1}^N w_{ij} (x_i - \bar{x})(x_j - \bar{x})}{(1/N) \sum_{i=1}^N (x_i - \bar{x})^2}, \quad (\text{S54})$$

where  $w_{ij}$  is 1 for neighboring agents  $i, j$  and  $W = \sum_{i=1}^N \sum_{j=1}^N w_{ij}$ . The  $\ell$ -ranged correlation  $\text{Corr}(X_n, X_{n+\ell})$  is an extended version of Moran's index and  $\ell = 1$  case that corresponds to the I on the ring topology. As shown in Fig. S3 (b),  $\text{Corr}(X_n, X_{n+\ell})$  eventually converges to 1 for small  $\ell$ . It shows regional convergence of wealth or income level  $x$  studied by [22–24]. However, for large  $\ell$ , correlation almost vanishes that means finite correlation length scale of the system. Interestingly, for the HBM model, significantly different long-range correlation patterns emerged by the configuration effect.

For the case of  $\mathcal{R} \simeq 0$ , the wealth-level correlation is restricted short-range and there is almost no correlation for large  $\ell$ . Thus,  $\text{Corr}(X_n, X_{n+\ell})$  becomes the U-shape. For the perfectly disassortative configuration ( $\mathcal{A}_{\min}$ ),  $\text{Corr}(X_n, X_{n+\ell})$  almost the same as the BM model and has uniform in the zero correlation region. The larger assortativity makes zero correlation region noisy but does not change macroscopic shape of  $\text{Corr}(X_n, X_{n+\ell})$ . However, for the case of  $\mathcal{R} > 0$ ,  $\text{Corr}(X_n, X_{n+\ell})$  becomes V-shape, and broad negative correlation region appears for large  $\ell$ . Because, for this case, the wealth-level regionally segregated and economic class of agents strongly depends on the position [see Fig. S6 (d) and Fig. S11].